

# 10

## Linear Induction Accelerators

The maximum beam energy achievable with electrostatic accelerators is in the range of 10 to 30 MeV. In order to produce higher-energy beams, the electric fields associated with changing magnetic flux must be used. In many high-energy accelerators, the field geometry is such that inductive fields cancel electrostatic fields over most the accelerator except the beamline. The beam senses a large net accelerating field, while electrostatic potential differences in the accelerating structure are kept to manageable levels. This process is called *inductive isolation*. The concept is the basis of linear induction accelerators [N. C. Christofilos *et. al.*, Rev. Sci. Instrum. **35**, 886 (1964)]. The main application of linear induction accelerators has been the generation of pulsed high-current electron beams.

In this chapter and the next we shall study the two major types of nonresonant, high-energy accelerators, the linear induction accelerator and the betatron. The principle of energy transfer from pulse modulator to beam is identical for the two accelerators; they differ mainly in geometry and methods of particle transport. The linear induction accelerator and betatron have the following features in common:

1. They use ferromagnetic inductors for broadband isolation.
2. They are driven by high-power pulse modulators.
3. They can, in principle, produce high-power beams.
4. They are both equivalent to a step-up transformer with the beam acting as the secondary.

## Linear Induction Accelerators

In the linear induction accelerator, the beam is a single turn secondary with multiple parallel primary inputs from high-voltage modulators. In the betatron, there is usually one pulsed-power primary input. The beam acts as a multi-turn secondary because it is wrapped in a circle.

The linear induction accelerator is treated first since operation of the induction cavity is relatively easy to understand. Section 10.1 describes the simplest form of inductive cavity with an ideal ferromagnetic isolator. Section 10.2 deals with the problems involved in designing isolation cores for short voltage pulses. The limitations of available ferromagnetic materials must be understood in order to build efficient accelerators with good voltage waveform. Section 10.3 describes more complex cavity geometries. The main purpose is to achieve voltage step-up in a single cavity. Deviations from ideal behavior in induction cavities are described in Sections 10.4 and 10.5. Subjects include flux forcing to minimize unequal saturation in cores, core reset for maximum flux swing, and compensation circuits to achieve uniform accelerating voltage. Section 10.6 derives the electric field in a complex induction cavity. The goal is to arrive at a physical understanding of the distribution of electrostatic and inductive fields to determine insulation requirements. Limitations on the average longitudinal gradient of an induction accelerator are also reviewed. The chapter concludes with a discussion of induction accelerations without ferromagnetic cores. Although these accelerators are of limited practical use, they make an interesting study in the application of transmission line principles.

### 10.1 SIMPLE INDUCTION CAVITY

We can understand the principle of an induction cavity by proceeding stepwise from the electrostatic accelerator. A schematic of a pulsed electrostatic acceleration gap is shown in Figure 10.1a. A modulator supplies a voltage pulse of magnitude  $V_0$ . The pulse is conveyed to the acceleration gap through one or more high-voltage transmission lines. If the beam particles have positive charge ( $+q$ ), the transmission lines carry voltage to elevate the particle source to positive potential. The particles are extracted at ground potential with kinetic energy  $qV_0$ . The energy transfer efficiency is optimized when the characteristic impedance of the generator and the parallel impedance of the transmission lines equals  $V_0/I$ . The quantity  $I$  is the constant-beam current. Note the current path in Figure 10.1a. Current flows from the modulator, along the transmission line center-conductors, through the beam load on axis, and returns through the transmission line ground conductor.

A major problem in electrostatic accelerators is controlling and supplying power to the particle source. The source and its associated power supplies are at high potential with respect to the laboratory. It is more convenient to keep both the source and the extracted beam at ground potential. To accomplish this, consider adding a conducting cylinder between the high-voltage and ground plates to define a toroidal cavity (Fig. 10.1h). The source and extraction point are at the same potential, but the system is difficult to operate because the transmission line output is almost

## Linear Induction Accelerators

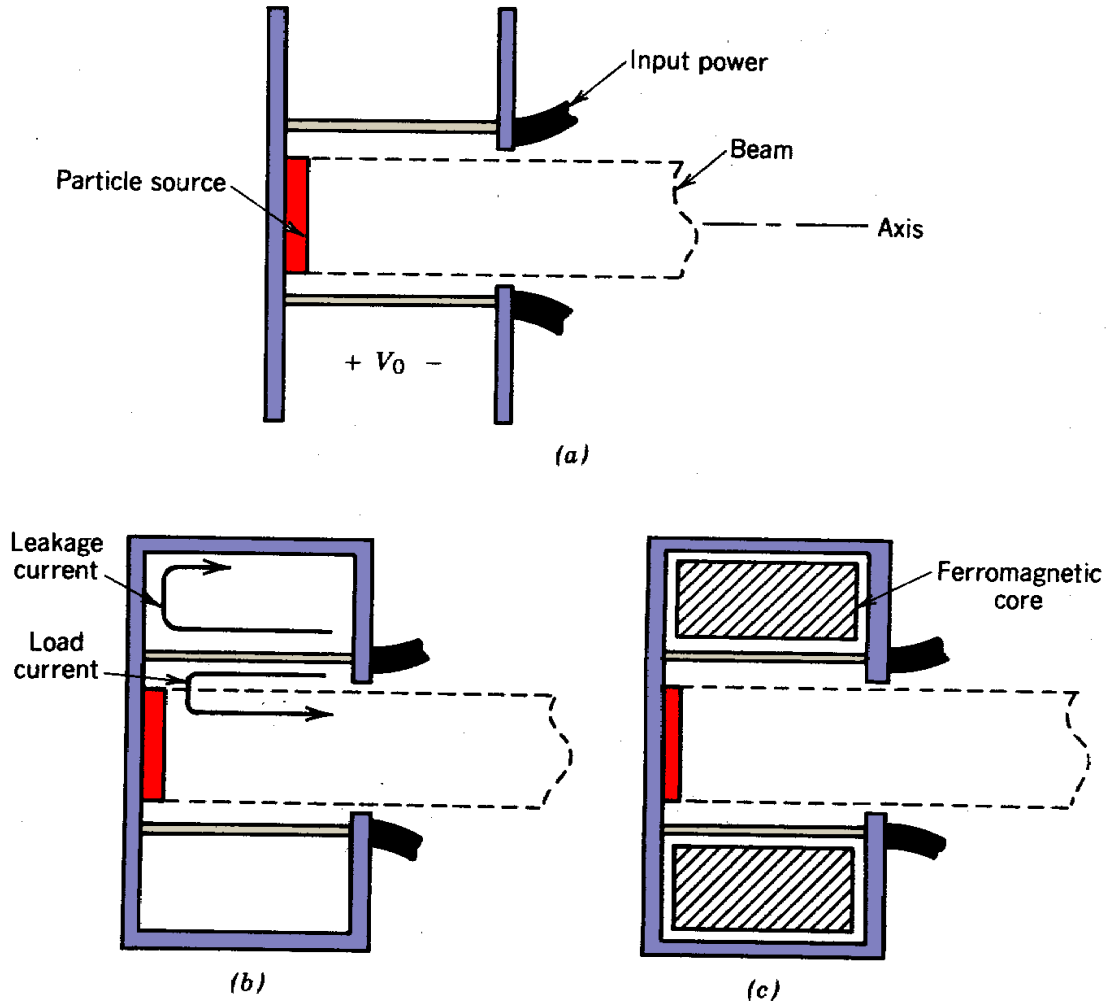


**Figure 10.1** Inductively isolated injector cavity. (a) Electrostatic injector. (b) Shorted electrostatic injector. (c) Injector with high-inductance leakage path.

short-circuited. Most of the current flows around the outer ground shield; this contribution is *leakage current*. There is a small voltage across the acceleration gap because the toroidal cavity has an inductance  $L_J$ . The leakage inductance is given by Eq. (9.15) if we take  $R_i$  as the radius of the power feeds and  $R_o$  as the radius of the cylinder. Thus, a small fraction of the total current flows in the load. The goal is clearly to reduce the leakage current compared to the load current; the solution is to increase  $L_J$ .

In the final configuration (Fig. 10.1c), the toroidal volume occupied by magnetic field from leakage current is filled with ferromagnetic material. If we approximate the ferromagnetic torus as an ideal inductor, the leakage inductance is increased by a factor  $\mu/\mu_o$ . This factor may exceed 1000. The leakage current is greatly reduced, so that most of the circuit current flows in the load. At constant voltage, the cavity appears almost as a resistive load to the pulse modulator. The voltage waveform is approximately a square pulse of magnitude  $V_0$  with some voltage droop

## Linear Induction Accelerators

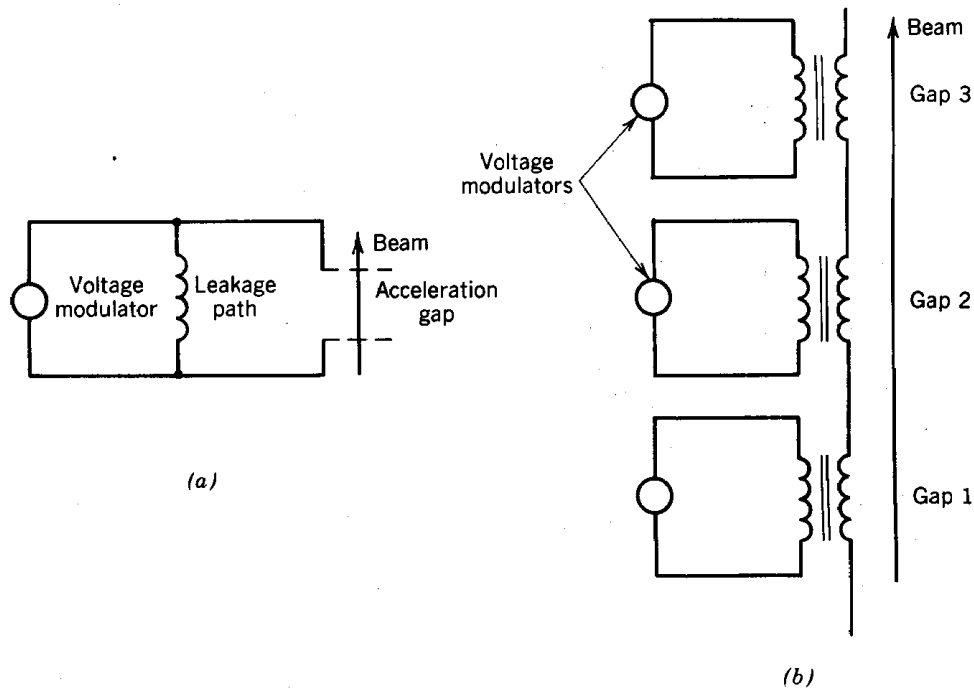


**Figure 10.2** Equivalent circuits. (a) Inductively isolated acceleration cavity. (b) Induction accelerator with a series of cavities.

caused by the linearly growing leakage current. The equivalent circuit model of the induction cavity is shown in Figure 10.2a; it is identical to the equivalent circuit of a 1:1 transformer (Fig. 9.7).

The geometry of Figure 10.1c is the simplest possible inductive linear accelerator cavity. A complete understanding of the geometry will clarify the operation of more complex cavities.

1. The load current does not encircle the ferromagnetic core. This means that the integral  $\int \mathbf{H} \cdot d\mathbf{l}$  from load current is zero through the core. In other words, there is little interaction between the load current and the core. The properties of the core set no limitation on the amount of beam current that can be accelerated.
2. To an external observer, both the particle source and the extraction point appear to be at ground potential during the voltage pulse. Nonetheless, particles emerge from the cavity with kinetic energy gain  $qV_0$ .
3. The sole purpose of the ferromagnetic core is to reduce leakage current.
4. There is an electrostaticlike voltage across the acceleration gap. Electric fields in the gap are identical to those we have derived for the electrostatic accelerator of Figure 10.1a. The inductive core introduces no novel accelerating field components.

## Linear Induction Accelerators

5. Changing magnetic flux generates inductive electric fields in the core. The inductive field at the outer radius of the core is equal and opposite to the electrostatic field; therefore, there is no net electric field between the plates at the outer radius, consistent with the fact that they are connected by a conducting cylinder. The ferromagnetic core provides inductive isolation for the cavity.

When voltage is applied to the cavity, the leakage current is small until the ferromagnetic core becomes saturated. After saturation, the differential magnetic permeability approaches  $\mu_0$  and the cavity becomes a low-inductance load. The product of voltage and time is limited. We have seen a similar constraint in the transformer [Eq. (9.29)]. If the voltage pulse has constant magnitude  $V_0$  and duration  $t_p$ , then

$$V_0 t_p = \Delta B A_c. \quad (10.1)$$

where  $A_c$  is the cross-sectional area of the core. The quantity  $\Delta B$  is the change of magnetic field in the core; it must be less than  $2B_s$ . Typical operating parameters for an induction cavity with a ferrite core are  $V_0 = 250$  kV and  $t_p = 50$  ns. Ferrites typically have a saturation field of 0.2-0.3 T. Therefore, the core must have a cross-sectional area greater than  $0.025$  m<sup>2</sup>.

The most common configuration for an inductive linear accelerator is shown in Figure 10.3. The beam passes through a series of individual cavities. There is no electrostatic voltage difference in

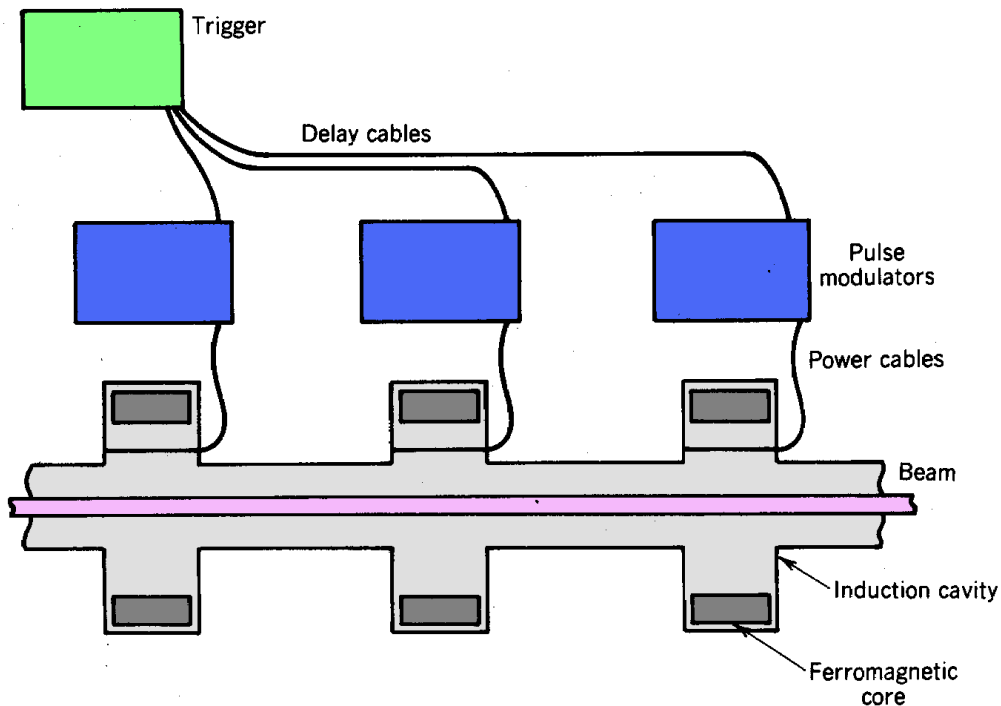


**Figure 10.3** Schematic diagram of a linear induction acceleration with cavities in series.

## Linear Induction Accelerators

**TABLE 10.1 Parameters of the ATA<sup>a</sup> Accelerator**

<i>Function</i>	
Research on the propagation of self-focused electron beams in gas, free electron laser driver.	
<i>Configuration</i>	
Length	85 m
Average gradient	0.59 MV/m
<i>Injector</i>	
Voltage	2.5 MV
Voltage source	10 stacked 250-kV induction cavities
Electron source diameter	0.25 m
Configuration	Triode, extraction by high-voltage control grid
Cathode	Cold cathode, whisker emission
<i>Main accelerator</i>	
Voltage gain	47.5 MeV
Voltage per stage	0.25 MV
Number of stages	190
Repetition rate	5 Hz 10 kHz (10 pulse burst)
<i>Acceleration cavity</i>	
Voltage	250 kV
Power modulator	Coaxial, water-filled Blumlein line pulse charged through a 10 : 1 step-up transformer
Modulator impedance	12 $\Omega$
Modulator switch	Gas-blown spark gap
Inductive isolator	Ferrite toroids
<i>Output beam</i>	
Pulselength	70 ns
Energy	50 MeV
Peak current	10 kA

<sup>a</sup> Advanced Test Accelerator, Lawrence Livermore Laboratory.

## Linear Induction Accelerators

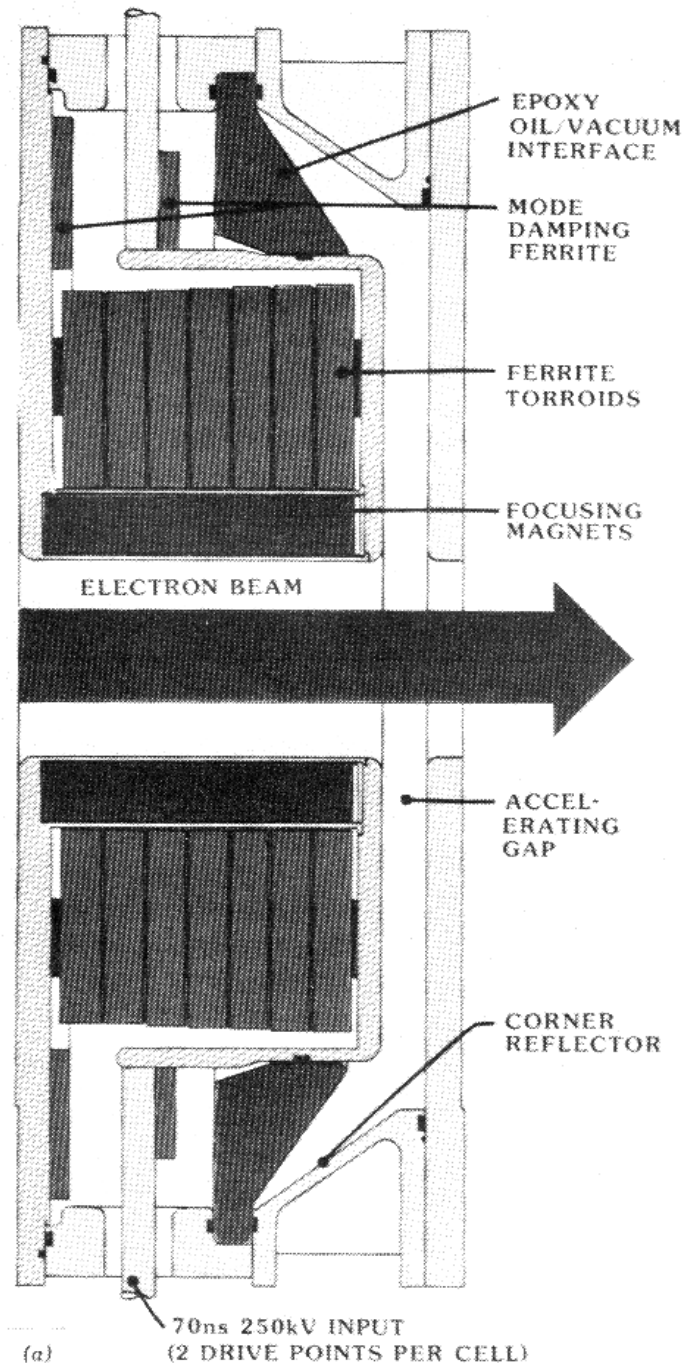


**Figure 10.4** Scale drawings, Advanced Test Accelerator. (a) 250 kV, ferrite isolated induction cell with mode damping ferrites to minimize beam breakup instabilities. (b) 2.5 MV, 10-cell block. (Courtesy D. Prono, Lawrence Livermore Laboratory.)



## Linear Induction Accelerators

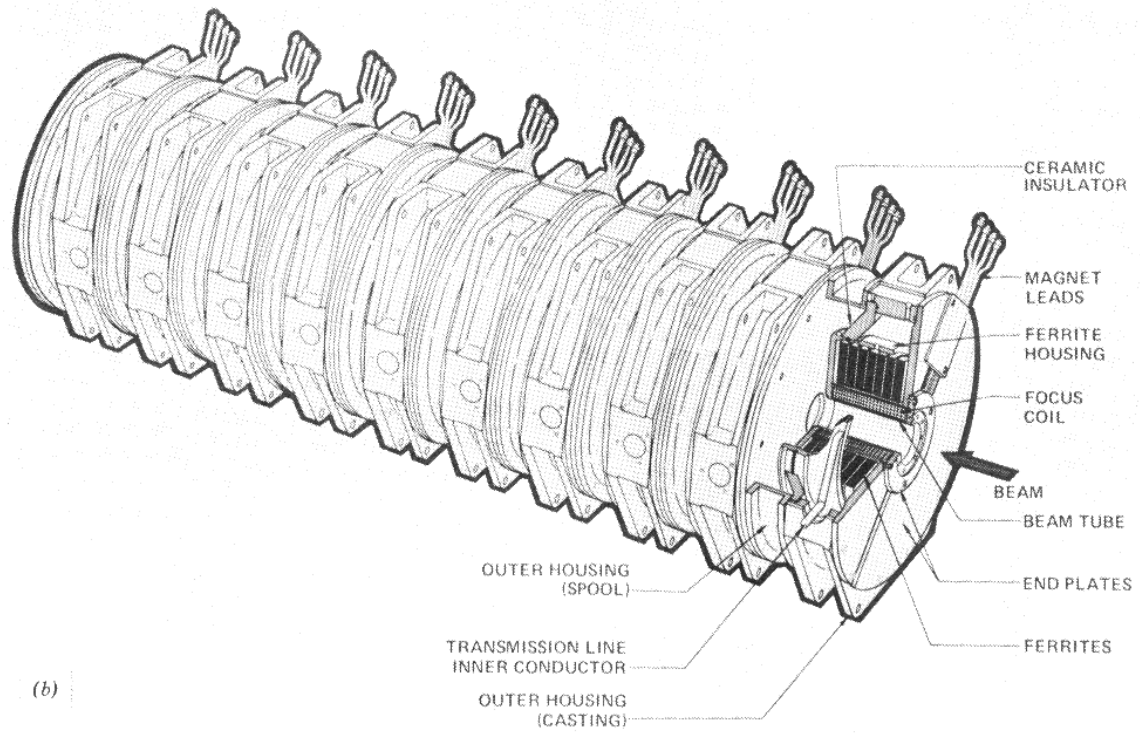


Figure 10.4 (Continued).



## Linear Induction Accelerators

the system higher than  $V_0$ . Any final beam energy consistent with cost and successful beam transport can be attained by adding more cavities. The equivalent circuit of an induction accelerator is shown in Figure 10.2b. Characteristics of the ATA machine, the highest energy induction accelerator constructed to date, are summarized in Table 10.1. A single-acceleration cavity and a 10-cavity block of the ATA accelerator are illustrated in Figures 10.4a and 10.4b, respectively.

### 10.2 TIME-DEPENDENT RESPONSE OF FERROMAGNETIC MATERIALS

We have seen in Section 5.3 that ferromagnetic materials have atomic currents that align themselves with applied fields. The magnetic field is amplified inside the material. The alignment of atomic currents is equivalent to a macroscopic current that flows on the surface of the material. When changes in applied field are slow, atomic currents are the dominant currents in the material. In this case, the magnetic response of the material follows the static hysteresis curve (Fig. 5.12).

Voltage pulse lengths in linear induction accelerators are short. We must include effects arising from the fact that most ferromagnetic materials are conductors. Inductive electric fields can generate real currents; real currents differ from atomic currents in that electrons move through the material. Real current driven by changes of magnetic flux is called *eddy current*. The contribution of eddy currents must be taken into account to determine the total magnetic fields in materials. In ferromagnetic materials, eddy current may prevent penetration of applied magnetic field so that magnetic moments in inner regions are not aligned. In this case, the response of the material deviates from the static hysteresis curve. Another problem is that resistive losses are associated with eddy currents. Depending on the type of material and geometry of construction, magnetic cores have a maximum usable frequency. At higher frequencies, resistive losses increase and the effective core inductance drops.

Eddy currents in inductive isolators and transformer cores are minimized by laminated core construction. Thin sheets of steel are separated by insulators. Most common ac cores are designed to operate at 60 Hz. In contrast, the maximum-frequency components in inductive accelerator pulses range from 1 to 100 MHz. Therefore, core design is critical for fast pulses. The frequency response is extended either by using very thin laminations or using alternatives to steel, such as ferrites.

The skin depth is a measure of the distance magnetic fields penetrate into materials as a function of frequency. We can estimate the skin depth in ferromagnetic materials in the geometry of Figure 10.5. A lamination of high  $\mu$  material with infinite axial extent is surrounded by a pulse coil excited by a step-function current waveform. The coil carries an applied current per length  $J_0$  (A/m) for  $t > 0$ . The applied magnetic field outside the high  $\mu$  material is

## Linear Induction Accelerators

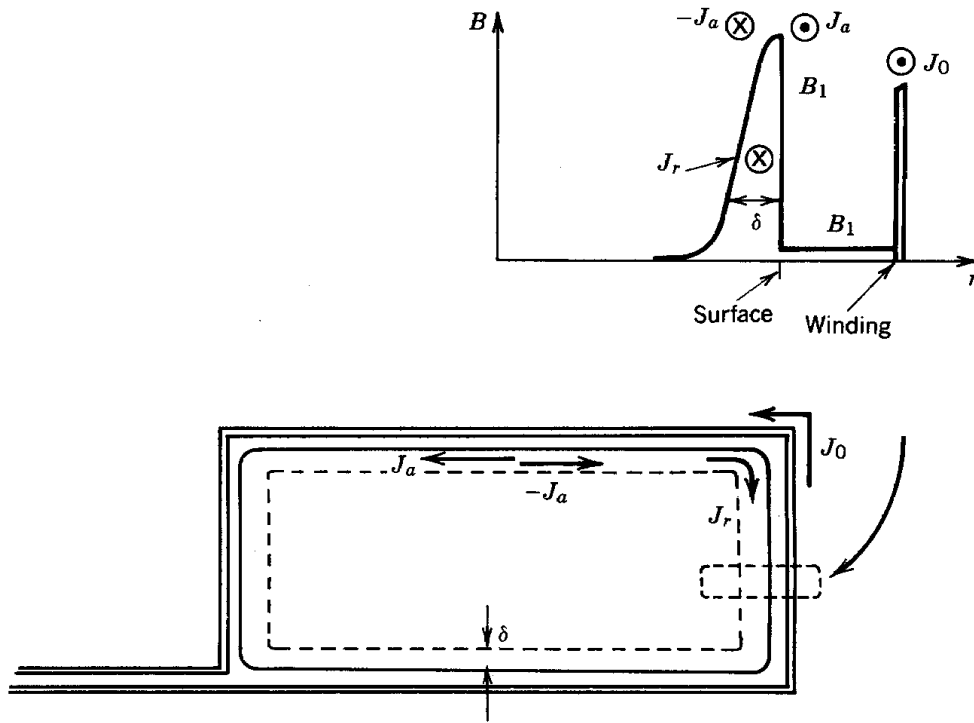


**Figure 10.5** Eddy currents and atomic currents in a ferromagnetic lamination subject to a pulsed external magnetic field.

$$B_1 = \mu_o J_o. \quad (10.2)$$

A real return current  $J_r$  flows in the conducting sample in the opposite direction from the applied current. We assume this current flows in an active layer on the surface of the material of thickness  $\delta$ . The magnetic field decreases across this layer and approaches zero inside the material. The total magnetic field as a function of depth in the material follows the variation of Figure 10.5. The return current is distributed through the active layer, while the atomic currents are concentrated at the layer surfaces. The atomic current  $J_a$  is the result of aligned dipoles in the region of applied magnetic field penetration; it amplifies the field in the active layer by a factor of  $\mu/\mu_o$ . The field just inside the material surface is  $(\mu/\mu_o)B_1$ . The magnetic field inward from the active layer is zero because the return current cancels the field produced by the applied currents. This implies that

$$J_r \approx -J_o. \quad (10.3)$$

We can estimate the skin depth by making a global balance between resistive effects (which impede the return current) and inductive effects (which drive the return current). The active, layer

## Linear Induction Accelerators

is assumed to penetrate a small distance into the lamination. The lamination has circumference  $C$ . If the material is an imperfect conductor with volume resistivity  $\rho$  ( $\Omega$ -m), the resistive voltage around the circumference from the flow of real current is

$$V_r \cong J_r \rho C / \delta. \quad (10.4)$$

The return current is driven by an electromotive force (emf) equal and opposite to  $V_r$ . The emf is equal to the rate of change of flux enclosed within a loop at the location under consideration. Because the peak magnetic field  $(\mu/\mu_o)B_1$  is limited, the change of enclosed flux must come about from the motion of the active layer into the material. If the layer moves inward a distance  $\delta$ , then the change of flux inside a circumferential loop is  $\Delta\Phi \cong (\mu/\mu_o)B_1 C \delta$ . Taking the time derivative and using Eq. (4.42), we find the inductive voltage

$$V_i \cong \mu C J_r (d\delta/dt).$$

Setting  $V_i$  equal to  $V_r$  gives

$$C \mu J_r (d\delta/dt) \cong J_r \rho C / \delta. \quad (10.5)$$

The circumference cancels out. The solution of Equation (10.5) gives the skin depth

$$\delta = \sqrt{2\rho t/\mu}. \quad (10.6)$$

The magnetic field moves into the material a distance proportional to the square root of time if the applied field is a step function. A more familiar expression for the skin depth holds when the applied field is harmonic,  $B_1 \sim \cos(\omega t)$ :

$$\delta = \sqrt{2\rho/\mu\omega} \quad (10.7)$$

In this case, the depth of the layer is constant; the driving emf is generated by the time variation of magnetic field.

The two materials commonly used in pulse cores are ferrites and steel. The materials differ mainly in their volume resistivity. Ferrites are ceramic compounds of iron-bearing materials with volume resistivity on the order of  $10^4 \Omega$ -m. Silicon steel is the most common transformer material. It is magnetically soft; the area of its hysteresis loop is small, minimizing hysteresis losses. Silicon steel has a relatively high resistivity compared to other steels,  $45 \times 10^{-8} \Omega$ -m. Nickel steel has a higher resistivity, but it is expensive. Recently, noncrystalline iron compounds

## Linear Induction Accelerators

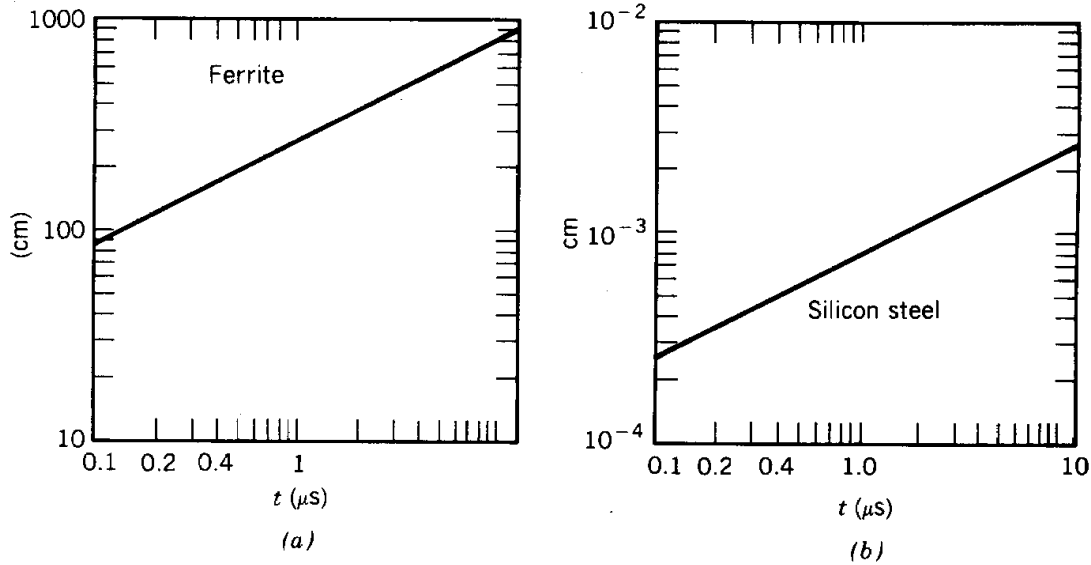


**Figure 10.6** Typical values of small-signal skin depth. (a) Ferrite. (b) Silicon steel.

have been developed. They are known by the tradename Metglas [Allied Corporation]. Metglas is produced in thin ribbons by injecting molten iron compounds onto a cooled, rapidly rotating drum. The rapid cooling prevents the formation of crystal structures. Metglas alloy 2605SC has a volume resistivity of  $125 \times 10^{-8} \Omega\text{-m}$ . Typical small-signal skin depths for silicon steel and ferrites as a function of applied field duration are plotted in Figure 10.6. There is a large difference between the materials; this difference is reflected in the construction of cores and the analysis of time-dependent effects.

An understanding of the time-dependent response of ferromagnetic materials is necessary to determine leakage currents in induction linear accelerators. The leakage current affects the efficiency of the accelerator and determines the compensation circuits necessary for waveform shaping. We begin with ferrites. In a typical ferrite isolated accelerator, the pulselength is 30-80 ns and the core dimension is  $< 0.5$  m. Reference to Figure 10.6 shows that the skin depth is larger than the core; therefore, to first approximation, we can neglect eddy currents and consider only the time variation of atomic currents. A typical geometry for a ferrite core accelerator cavity is shown in Figure 10.7. The toroidal ferrite cores are contained between two cylinders of radii  $R_i$  and  $R_o$ . The leakage current circuit approximates a coaxial transmission line filled with high  $\mu$  material. The transmission line has length  $d$ ; it is shorted at the end opposite the pulsed power input. We shall analyze the transmission line behavior of the leakage current circuit with the assumption that  $(R_o - R_i)/R_o \ll 1$ . Radial variations of toroidal magnetic field in the cores are neglected.

The transmission line of length  $d$  has impedance  $Z_c$  given by Eq. (9.86) and a relatively long transit time  $\delta t = d\sqrt{\epsilon\mu}$ . Consider, first, application of a low-voltage step-function pulse. A voltage wave from a low-impedance generator of magnitude  $V_o$  travels through the core at velocity  $c/\sqrt{(\epsilon/\epsilon_o)(\mu/\mu_o)}$  carrying current  $V_o/Z_c$ . The wave is reflected at time  $\Delta t$  with inverse

## Linear Induction Accelerators

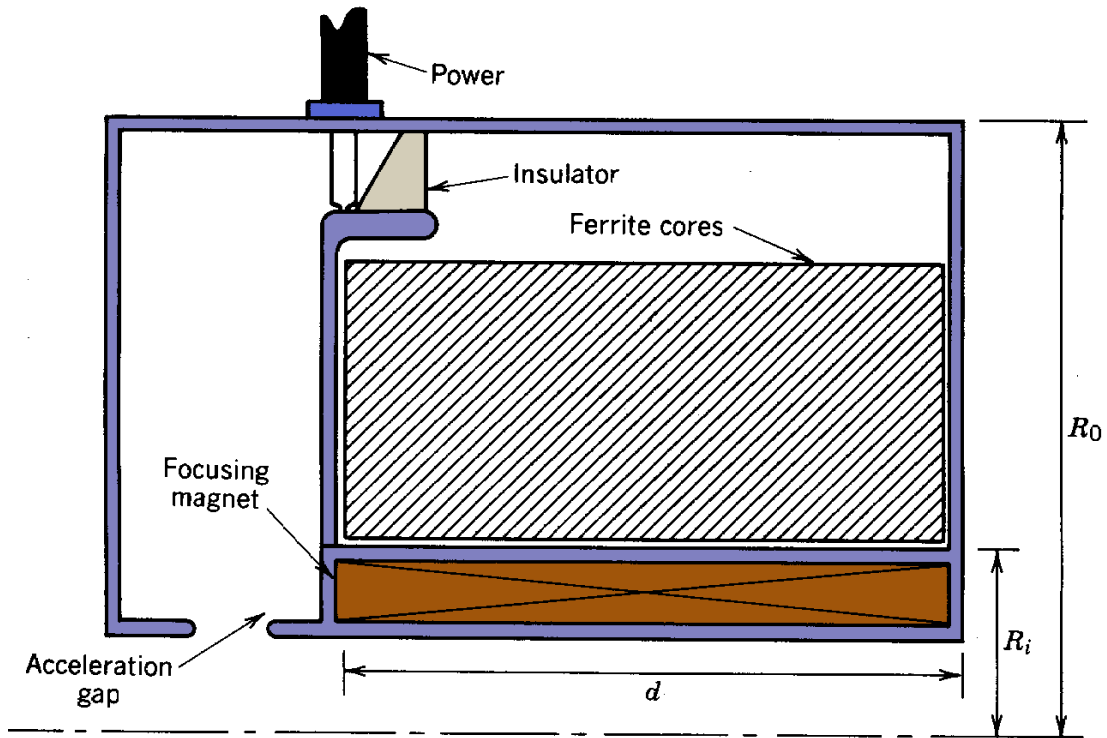


**Figure 10.7** Geometry of an idealized ferrite core acceleration cavity.

polarity from the short-circuit termination. The inverted wave arrives back at the input at time

$2\Delta t$ . In order to match the input voltage, two voltage waves, each carrying current  $V_0/Z_c$  are launched on the line. The net leakage current during the interval  $2\Delta t \leq t \leq 4\Delta t$  is  $3V_0/Z_c$ . Subsequent wave reflections result in the leakage current variation illustrated in Figure 10.8a. The dashed line in the figure shows the current corresponding to an ideal lumped inductor with  $L = Z_c\Delta t$ . The core approximates a lumped inductor in the limit of low voltage and long pulse length. The leakage current diverges when it reaches the value  $i_s = 2\pi R_i H_s$ . The quantity  $H_s$  is the saturation magnetizing force.

Next, suppose that the voltage is raised to  $V_s$  so that the current during the initial wave transit is

$$i = V_s/Z_c = i_s = 2\pi R_i H_s. \quad (10.8)$$

The wave travels through the core at the same velocity as before. The main difference is that the magnetic material behind the wavefront is saturated. When the wave reaches the termination at time  $\Delta t$ , the entire core is saturated. Subsequently, the leakage circuit acts as a vacuum transmission line. The quantities  $Z_c$  and  $\Delta t$  decrease by a factor of  $\mu/\mu_0$ , and the current increases rapidly as inverted waves reflect from the short circuit. The leakage current for this case is plotted in Figure 10.8b. The volt-second product before saturation again satisfies Eq. (10.1).

At higher applied voltage, electromagnetic disturbances propagate into the core as a saturation

## Linear Induction Accelerators

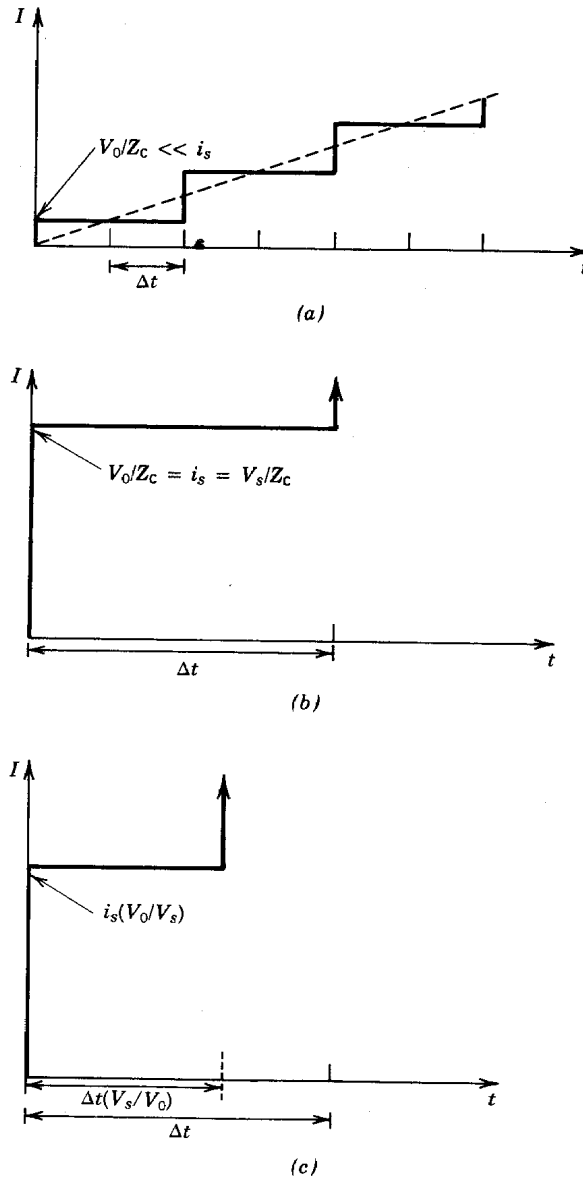


**Figure 10.8** Time-dependent leakage current in a ferrite core acceleration cavity. (a) Low applied voltage. (b) Saturation voltage. (c) High voltage.

wave. The wave velocity is controlled by the saturation of magnetic material in the region of rising current; the saturation wave moves more rapidly than the speed of electromagnetic pulses in the high  $\mu$  medium. When  $V_0 > V_s$  conservation of the volt-second product implies that the time  $T$  for the saturation wave to propagate through the core is related to the small-signal propagation time by

$$T/\Delta t = V_s/V_0. \quad (10.9)$$

## Linear Induction Accelerators

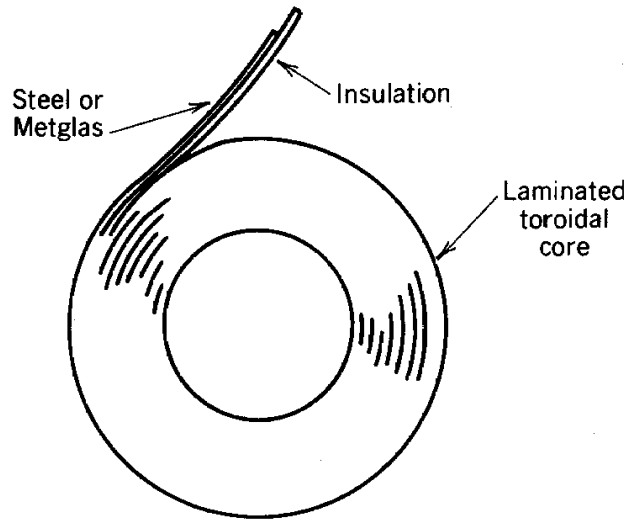


**Figure 10.9** Construction of a laminated ferromagnetic isolation core.

The transmission line is charged to voltage  $V_0$  at time  $T$ ; therefore, a charge  $CV_0$  flowed into the leakage circuit where  $C$  is the total capacitance of the circuit. The magnitude of the leakage current accompanying the saturation wave is thus  $i = CV_0/T$ , or

$$i = i_s (V_0/V_s). \quad (10.10)$$

The leakage current exceeds the value given in Eq. (10.8). Leakage current variation in the high-voltage limit is illustrated in Figure 10.8c.

In contrast to ferrites, the skin depth in steel or Metglas is much smaller than the dimension of the core. The core must therefore be divided into small sections so that the magnetic field penetrates the material. This is accomplished by laminated construction. Thin metal ribbon is wound on a cylindrical mandrel with an intermediate layer of insulation. The result is a toroidal core (Fig. 10.9). In subsequent analyses, we assume that the core is composed of nested cylinders and that there is no radial conduction of real current. In actuality, some current flows from the inside to the outside along the single ribbon. This current is very small because the path has a huge inductance. A laminated pulse core may contain thousands of turns.

Laminated steel cores are effective for pulses in the microsecond range. In the limit that  $(R_o - R_i)/R_o \ll 1$ , the applied magnetic field is the same at each lamination. The loop voltage around a lamination is thus  $V_0/N$ , where  $N$  is the number of layers. In an actual toroidal core, the applied field is proportional to  $1/r$  so that lamination voltage is distributed unevenly; we will consider the consequences of flux variation in Section 10.4.

If the thickness of the lamination is less than the skin depth associated with the pulselength, then magnetic flux is distributed uniformly through a lamination. Even in this limit, it is difficult to calculate the inductance exactly because the magnetic permeability varies as the core field changes from  $-B_s$  to  $B_s$ . For a first-order estimate of the leakage current, we assume an average



## Linear Induction Accelerators

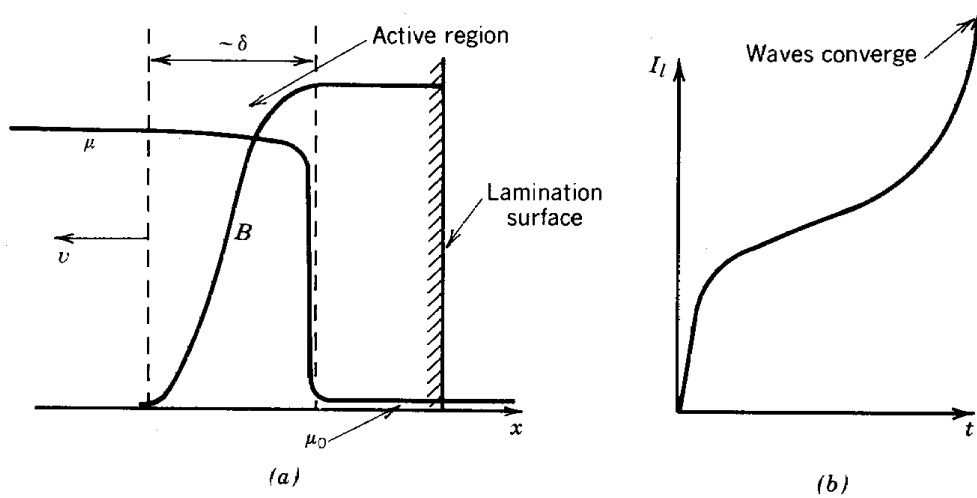


**Figure 10.10** Saturation waves in a laminated ferromagnetic core. (a) Spatial variation of magnetic field and  $\mu$  in a lamination. (b) Time variation of leakage current.

permeability  $\bar{\mu} = B_s/H_s$ . The inductance of the core is

$$L = \bar{\mu} d \ln(R_o/R_i) / 2\pi. \quad (10.11)$$

The time-dependent leakage current is

$$i_l \cong (V_o/L) t = [2\pi V_o \bar{\mu} d \ln(R_o/R_i)] t. \quad (10.12)$$

The behavior of laminated cores is complex for high applied voltage and short pulselength. When the skin depth is less than half the lamination thickness, magnetic field penetrates in a saturation wave (Fig. 10.10a). There is an active layer with large flux change from atomic current alignment. There is a region behind the active layer of saturated magnetic material; the skin depth for field penetration is large in this region because  $\mu \cong \mu_o$ . Changes in the applied field are communicated rapidly through the saturated region. The active layer moves inward, and the saturation wave converges at the center at a time equal to the volt-second product of the lamination divided by  $V_o/N$ .

Although the volt-second product is conserved in the saturation wave regime, the inductance of the core is reduced below the value given by Eq. (10.11). This comes about because only a fraction of the lamination cross-sectional area contributes to flux change at a particular time. The core inductance is reduced by a factor on the order of the width of the active area divided by the half-width of the lamination. Accelerator efficiency is reduced because of increased leakage current and eddy current core heating. Leakage current in the saturation wave regime is illustrated in Figure 10.10b.

**TABLE 10.2 Properties: Materials for Induction Linear Accelerators**

Quantity	Ferrite (TDK PE-14)	Silicon Steel	Metglas Allied (2605SC)
$\rho$ ( $\Omega\text{-m}$ )	$10^4$	$45 \times 10^{-8}$	$125 \times 10^{-8}$
$\mu/\mu_0$ (small signal)	300–600	600	1200
$\langle(\mu/\mu_0)\rangle$ $B_s/\mu_0 H_s$ (static)		$10^4$	$10^5$
$B_s$ (T)	0.4	1.4	1.6
$B_r$ (T)	0.3	1.2	1.4
$\Delta B_{\text{max}}$ (T)	0.7	2.6	3.0

Core material and lamination thickness should be chosen so that skin depth is greater than half the thickness of the lamination. If this is impossible, the severity of leakage current effects can best be estimated by experimental modeling. Saturation wave analyses seldom give an accurate figure for leakage current. Measurements for a single lamination are simple; a loop around the lamination is driven with a pulse of voltage  $V_0/N$  and pulselength equal to that of the accelerator. The most reliable method to include the effects of radial field variations is to perform measurements on a full-radius core segment.

Properties of common magnetic materials are listed in Table 10.2. Ferrite cores have the capability for fast response; they are the only materials suitable for the 10-50 ns regime. The main disadvantages of ferrites are that they are expensive and that they have a relatively small available flux swing. This implies large core volumes for a given volt-second product.

Silicon steel is inexpensive and has a large magnetic field change,  $\sim 3$  T. On the other hand, it is a brittle material and cannot be wound in thicknesses  $< 2$  mil ( $5 \times 10^{-3}$  cm). Reference to Figure 10.6 shows that silicon steel cores are useful only for pulselengths greater than  $1 \mu\text{s}$ . There has been considerable recent interest in Metglas for induction accelerator cores. Metglas has a larger volume resistivity than silicon steel. Because of the method of its production, it is available in uniform thin ribbons. It has a field change about equal to silicon steel, and it is expected to be fairly inexpensive. Most important, because it is noncrystalline, it is not brittle and can be wound into cores in ribbons as thin as 0.7 mil ( $1.8 \times 10^{-3}$  cm). It is possible to construct Metglas cores for short voltage pulses. If there is high load current and leakage current is not a primary concern, Metglas cores can be used for pulses in the 50-ns range.

The distribution of electric field in isolation cores must be known to determine insulation requirements. Electric fields have a simple form in laminated steel cores. Consider the core in the cavity geometry of Figure 10.11 with radial variations of applied field neglected. We know that there is a voltage  $V_0$  between the inner and outer cylinders at the input end (marked  $\alpha$ ) and there is zero voltage difference on the right-hand side (marked  $\beta$ ) because of the connecting radial

## Linear Induction Accelerators

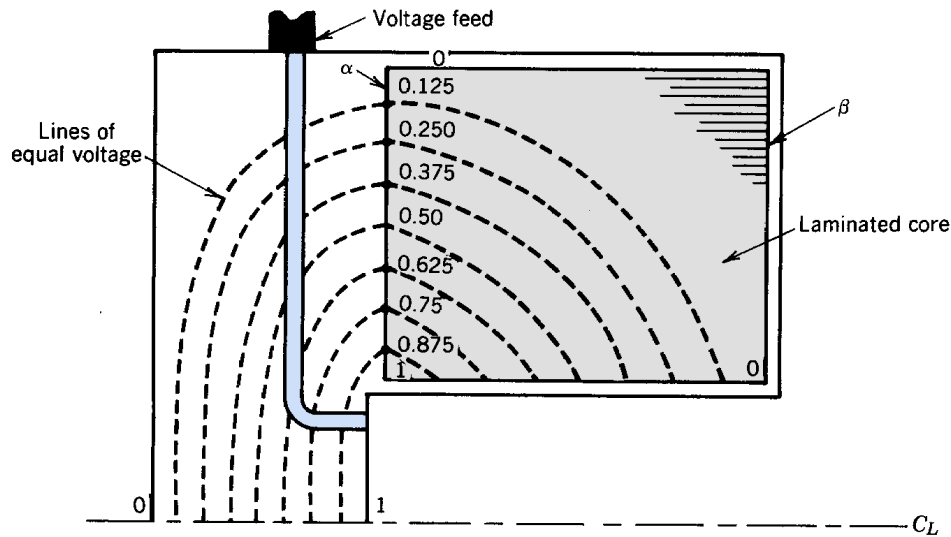


**Figure 10.11** Distribution of voltage in a laminated isolation core (no local saturation).

conductor. Furthermore, the laminated core has zero conductivity in the radial direction but has high conductivity in the axial direction. Image charge is distributed on the laminations to assure that  $E_z$  equals zero along the surfaces. Therefore, the electric field is almost purely radial in the core. This implies that:

1. Except for small fringing fields, the electric field is radial along the input edge ( $\alpha$ ). The voltage drop across each insulating layer on the edge is  $V_0/N$ .
2. Moving into the core, inductive electric fields cancel the electrostatic fields. The net voltage drop across the insulating layers decreases linearly to zero moving from  $\alpha$  to  $\beta$ .

Figure 10.11 shows voltage levels in the core relative to the outer conductor. Note that this is not an electrostatic plot; therefore, the equal voltage lines in the core are not normal to the electric fields.

### 10.3 VOLTAGE MULTIPLICATION GEOMETRIES

Inductive linear accelerator cavities can be configured as step-up transformers. High-current, moderate-voltage modulators can be used to drive a lower-current beam load at high voltage. Step-up cavities are commonly used for high-voltage electron beam injectors. Problems of beam transport and stability in subsequent acceleration sections are reduced if the injector voltage is high. Multi-MV electrostatic pulse generators are bulky and difficult to operate, but 0.25-MV modulators are easy to design. The inductive cavity of Figure 10.12a uses 10 parallel 0.25-MV

## Linear Induction Accelerators

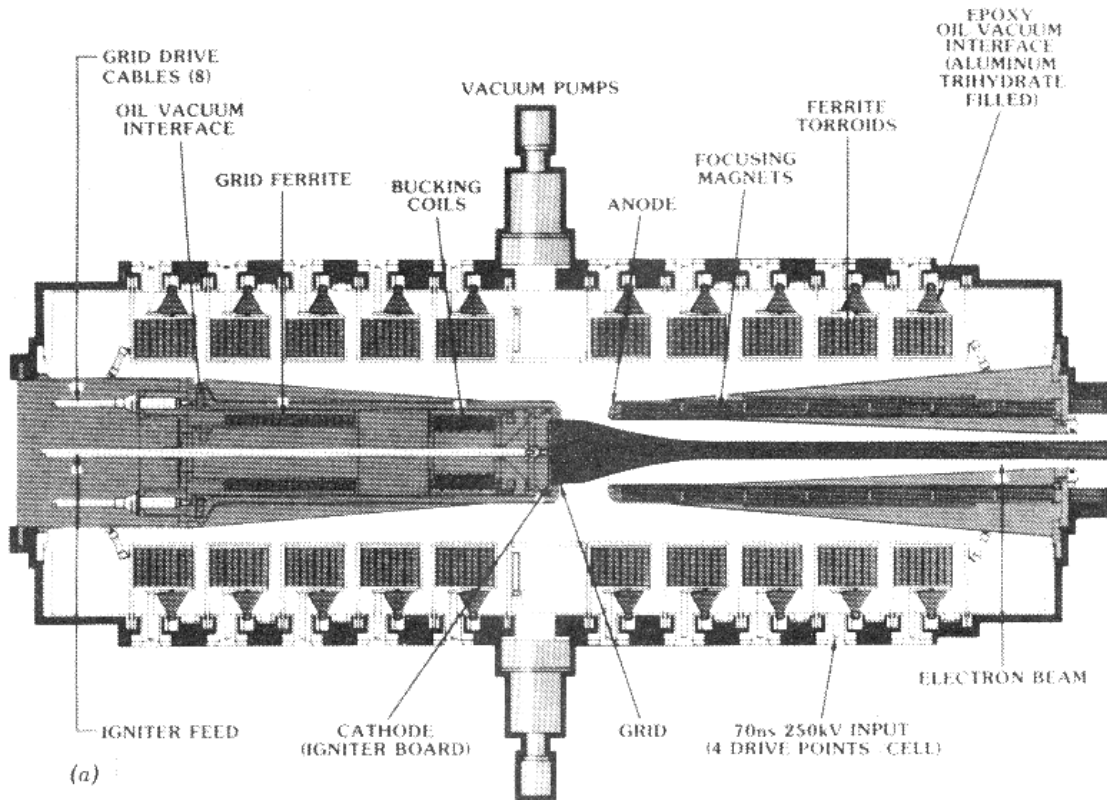


Figure 10.12 Longitudinal stacking of induction cells for electron injection high energy. (a) Scale drawing of ATA 2.5-MeV injector, Advanced Test Accelerator. (Courtesy D. Prono, Lawrence Livermore Laboratory.) (b) Current flow in a four-stage cavity.

## Linear Induction Accelerators

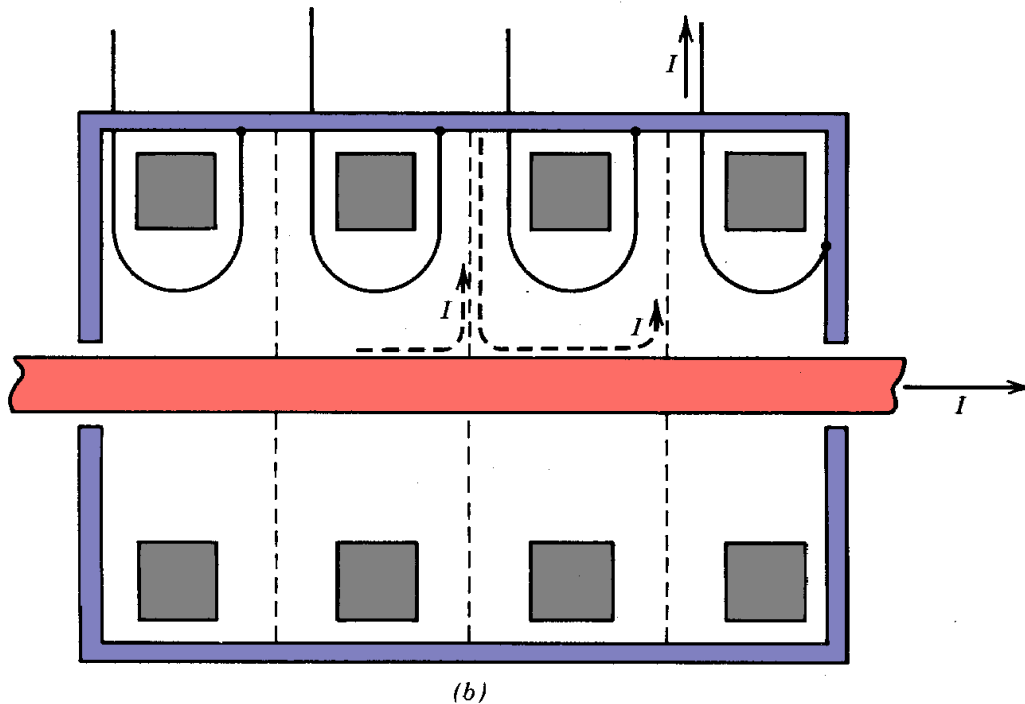


Figure 10.12 (Continued).

pulses to generate a 2.5-W pulse across an injection gap. Figure 10.12 illustrates *longitudinal core stacking*.

A schematic view of a 4:1 step-up circuit with longitudinal stacking is shown in Figure 10.12b. Note that if electrodes are inserted at the positions of the dotted lines, the single gap of Figure 10.12b is identical to a four-gap linear induction accelerator. The electrodes carry no current, so that the circuit is unchanged by their presence. We assume that the four input transmission lines of characteristic impedance  $Z_0$  carry pulses with voltage  $V_0$  and current  $I_0 = V_0/Z_0$ . A single modulator to drive the four lines must have an impedance  $4Z_0$ . The high core inductance constrains the net current through the axis of each core to be approximately zero. Therefore, the beam current for a matched circuit is  $I_0$ . The voltage across the acceleration gap is  $4V_0$ . The matched load impedance is therefore  $4Z_0$ . This is a factor of 16 higher than the primary impedance, as we expect for a 4:1 step-up transformer.

It is also possible to construct voltage step-up cavities with radial core stacking, as shown in Figure 10.13. It is more difficult to understand the power flow in this geometry. For clarity, we will proceed one step at a time, evolving from the basic configuration of Figure 10.1c to a dual-core cavity. We assume the beam load is driven by matched transmission lines. There are two main constraints if the leakage circuits have infinite impedance: (1) all the current in the system must be accounted for and (2) there is no net axial current through the centers of either of the cores.

## Linear Induction Accelerators

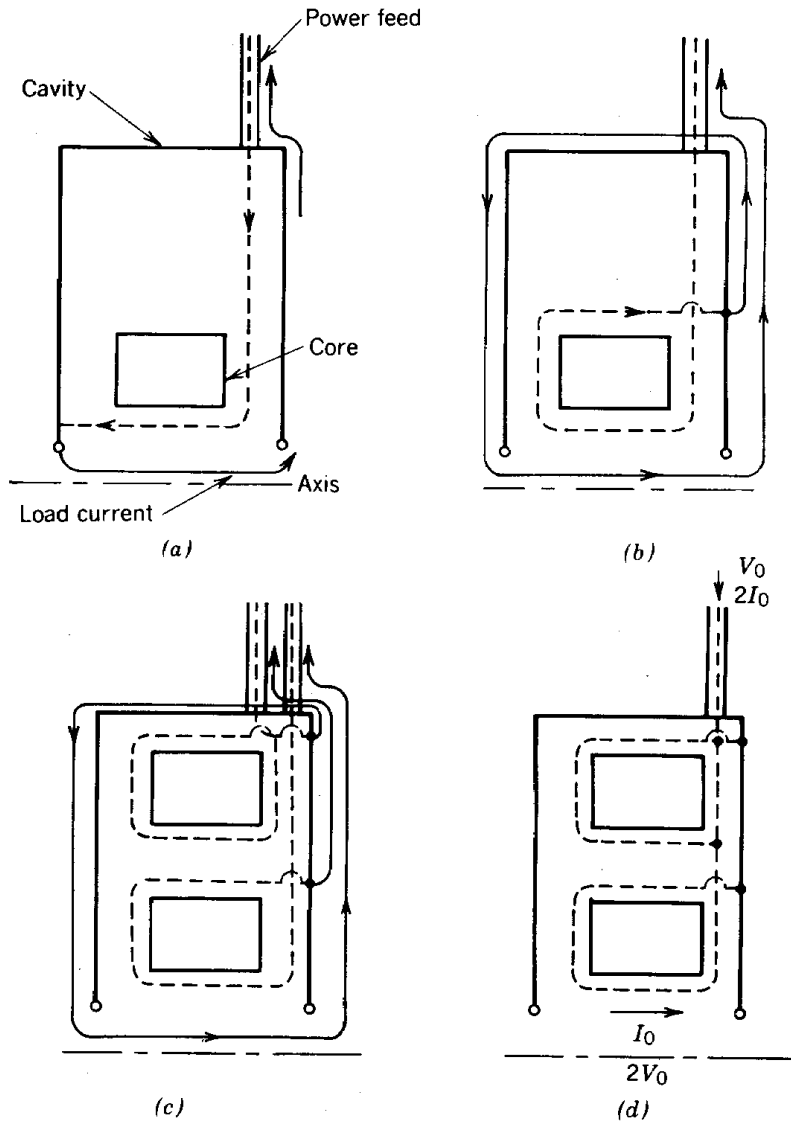


**Figure 10.13** Acceleration cavity with radially stacked cores. Dashed arrows, current on power feeds; solid arrows, current in cavity. (a) Single core, simple power feed. (b) Single core with encircling power feed. (c) Two cores with dual power feeds. (d) Two cores with single power feed and flux-forcing connections.

Figure 10.13a shows a cavity with one core and one input transmission line. The difference from Figure 10.1c is that the line enters radially; this feature does not affect the behavior of the cavity. Note the current path; the two constraints are satisfied. In Figure 10.13b, the power lead is wrapped around the core and connected back to the input side of the inductive cavity. The current cannot flow outward along the wall of the cavity and return immediately along the transmission line outer conductor; this path has high inductance. Rather, the current follows the convoluted path shown, flowing through the on-axis load before returning along the ground lead

## Linear Induction Accelerators

of the transmission line. Although the circuit of Figure 10.13b has a more complex current path and higher parasitic inductance than that of Figure 10.12a, the net behavior is the same.

The third step is to add an additional core and an additional transmission line with power feed wrapped around the core. The voltage on the gap is  $2V_0$  and the load current is equal to that from one line. Current flow from the two lines is indicated. The current paths are rather complex; current from the first transmission line flows around the inner core, along the cavity wall, and returns through the ground conductor of the second line. The current from the second line flows around the cavity, through the load, back along the cavity wall, and returns through the ground lead of the first line. The cavity of Figure 10.13c conserves current and energy. Furthermore, inspection of the current paths shows that the net current through the centers of both cores is zero. An alternative configuration that has been used in accelerators with radially stacked cores is shown in Figure 10.13d. Both cores are driven by a single-input transmission line of impedance  $V_0/2I_0$ .

## 10.4 CORE SATURATION AND FLUX FORCING

In our discussions of laminated inductive isolation cores, we assumed that the applied magnetic field is the same at all laminae. This is not true in toroidal cores where the magnetic field decreases with radius. Three problems arise from this effect:

1. Electric fields are distributed unevenly among the insulation layers. They are highest at the center of the core.
2. The inner layers reach saturation before the end of the voltage pulse. There is a global saturation wave in the core; the region of saturation grows outward. The result is that the magnetically active area of the core decreases following saturation of the inner lamination. The inductance of the isolation circuit drops at the end of the pulse.
3. During the saturation wave, the circuit voltage is supported by the remaining unsaturated laminations. The field stress is highly nonuniform so that insulation breakdowns may occur.

The first problem can be addressed by using thicker insulation near the core center. The second and third problems are more troublesome, especially in accelerators with radially stacked cores. The effects of unequal saturation on the leakage current and cavity voltage are illustrated in Figure 10.14. The leakage current grows non-linearly during the latter portion of the pulse making compensation (Section 10.5) difficult. The tail end of the voltage pulse droops. Although the quantity  $\int V dt$  is conserved, the waveform of Figure 10.14 may be useless for acceleration if a small beam energy spread is required.



## Linear Induction Accelerators

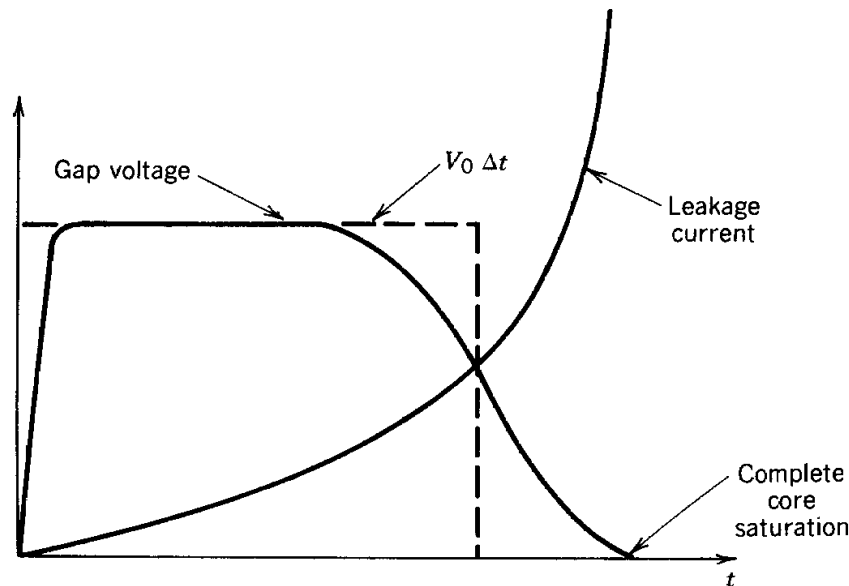


**Figure 10.14** Acceleration gap voltage and leakage current waveforms with local saturation of isolation cores.

The problem of unequal saturation could be solved by using a large core to avoid saturation of the inner laminations. This approach is undesirable because core utilization is inefficient. The core volume and cost increase and the average accelerating gradient drops (see Section 10.7). Ideally, the core and cavity should be designed so that the entire volume of the core reaches saturation simultaneously at the end of the voltage pulse. This condition can be approached through *flux forcing*.

Flux forcing was originally developed to equalize saturation in large betatron cores. We will illustrate the process in a two-core radially stacked induction accelerator cavity. In Figure 10.15a, two open conducting loops encircle the cores. There is an applied voltage pulse of magnitude  $V_0$ . The voltage between the terminals of the outer loop is smaller than that of the inner loop because the enclosed magnetic flux change is less. The sum of the voltages equals  $V_0$  with polarities as shown in the figure. In Figure 10.14b, the ends of the loops are connected together to form a single figure-8 winding. If the net enclosed magnetic flux in the outer loop were smaller than that of the inner loop, a high current would flow in the winding. Therefore, we conclude that a moderate current is induced in the winding that equalizes the magnetic flux enclosed by the two loops.

The figure-8 winding is called a *flux-forcing strap*. The distribution of current is illustrated in Figure 10.15c. The inner loop of the flux-forcing strap reduces the magnetic flux in the inner core, while the outer loop current adds flux at the outer core. If both cores in Figure 10.15 have the same cross-sectional area, they reach saturation at the same time because  $d\Phi/dt$  is the same inside both loops. Of course, local saturation can still occur in a single core. Nonetheless, the severity of saturation is reduced for two reasons:

## Linear Induction Accelerators

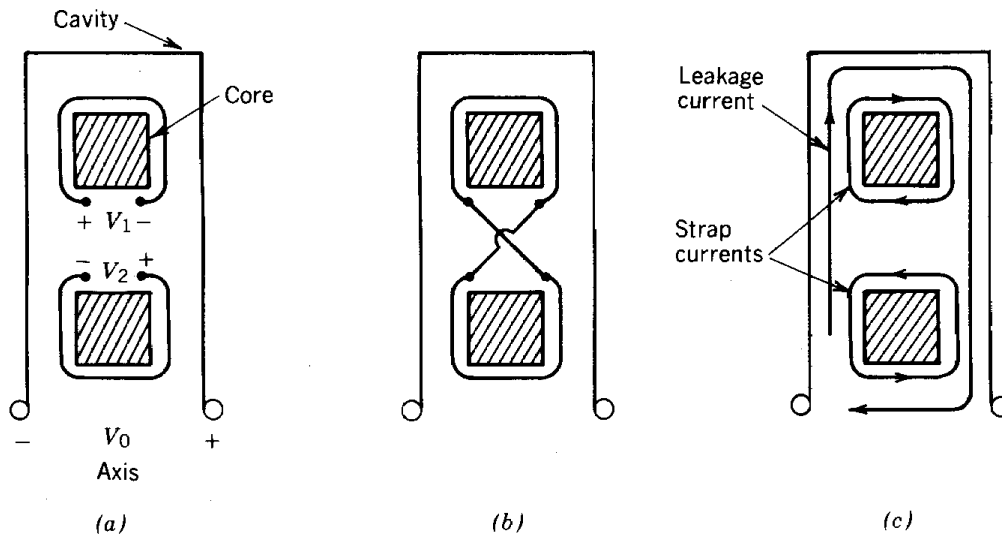


**Figure 10.15** Flux-forcing straps. (a) Voltage on unconnected straps. (b) Figure-8 winding for flux forcing. (c) Current flow in flow-forcing straps relative to leakage current.

1. The ratio of the inner to outer radius is closer to unity for a single core section than for the entire stack.
2. Even if there is early saturation at the inside of the inner core, the drop in leakage circuit inductance is averaged over the stack.

Figure 10.16 illustrates an induction cavity with four core sections. The cavity was designed to achieve a high average longitudinal gradient in a long pulse linear induction accelerator. A large-diameter core stack was used for high cross-sectional area. There are two interesting aspects of the cavity:

1. The cores are driven in parallel from a single-pulse modulator. There is a voltage step-up by a factor of 4.

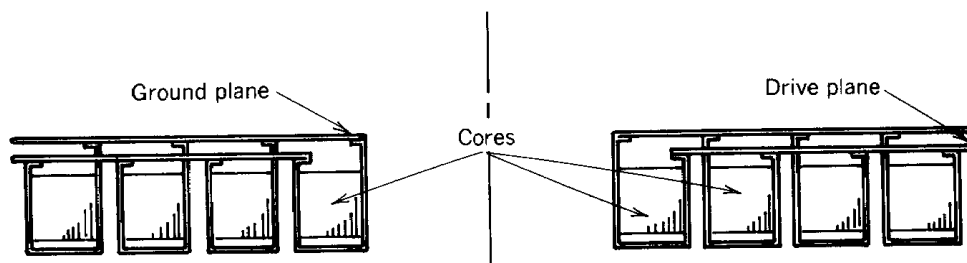


**Figure 10.16** Core and power feed geometry for a 4:1 step-up cavity with flux forcing. (Courtesy M. Wilson, National Bureau of Standards.)

## Linear Induction Accelerators

2. The parallel drive configuration assures that the loop voltage around each core is the same; therefore, the current distribution in the driving loops provides automatic flux forcing.

### 10.5 CORE RESET AND COMPENSATION CIRCUITS

Following a voltage pulse, the ferromagnetic core of an inductive accelerator has magnetic flux equal to  $+B_r$ . The core must be reset to  $-B_r$  before the next pulse; otherwise, the cavity will be short-circuited soon after the voltage is applied.

Reverse biasing of the core is accomplished with a reset circuit. The reset circuit must have the following characteristics:

1. The circuit can generate an inverse voltage-time product greater than  $(B_s + B_r) A_c$ .
2. It can supply a unidirectional reverse current through the core axis of magnitude

$$I_s > 2\pi R_o H_s. \quad (10.13)$$

The quantity  $H_s$  is the magnetizing force of the core material and  $R_o$  is the outercore radius. Higher currents are required for fast-pulsed reset.

3. The reset circuit has high voltage isolation so that it does not absorb power during the primary pulse.

A long pulse induction cavity with reset circuit is shown in Figure 10.17. Note that a *damping resistor* in parallel with the beam load is included in the cavity. Damping resistors are incorporated in most induction accelerators. Their purpose is to prevent overvoltage if there is an error in beam arrival time. Some of the available modulator energy is lost in the damping resistor. Induction cavities have typical energy utilization efficiencies of 20-50%.

Reset is performed by an RC circuit connected to the cavity through a mechanical high-voltage relay. The relay acts as an isolator and a switch. The reset capacitor  $C_r$  is charged to voltage  $-V_r$ ; the reset resistance  $R_r$  is small compared to the damping resistor  $R_d$ . There is an inductance  $L_r$  associated with the flow of reset current. Neglecting  $L_r$  and the current through the leakage circuit, the first condition above is satisfied if

$$\int V_r \exp(-t/R_d C_r) dt > (B_s + B_r) A_c. \quad (10.14)$$

If the inequality of Eq. (10.14) is well satisfied, the second condition is fulfilled if

$$V_r/R_d > I_s. \quad (10.15)$$

## Linear Induction Accelerators

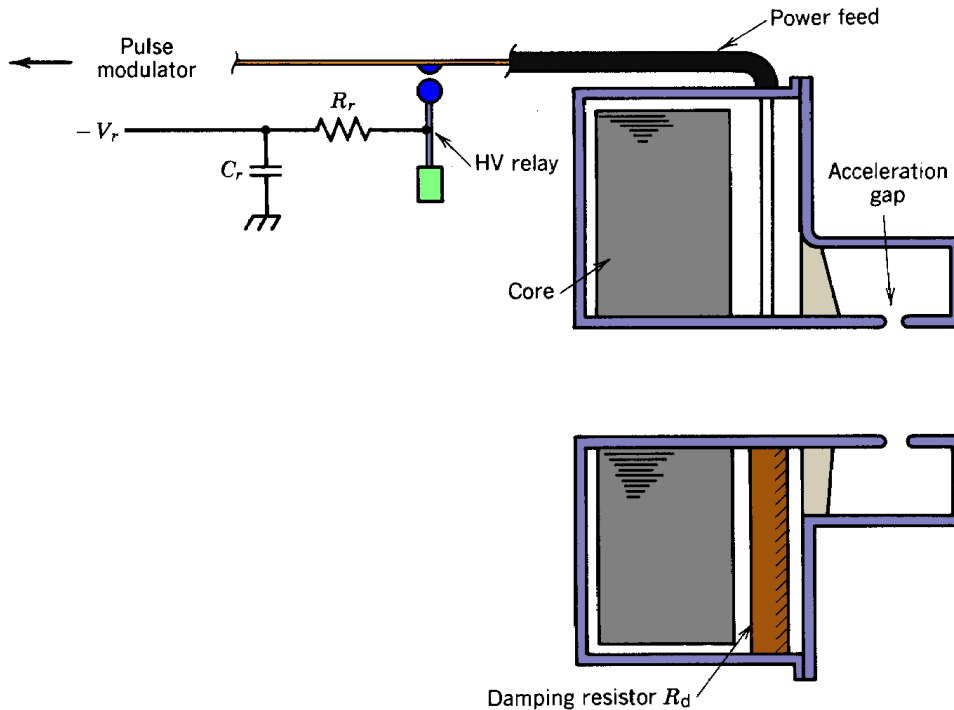


**Figure 10.17** Reset circuit for a long-pulse induction cavity.

Equation (10.15) implies that the reset resistance should be as low as possible. There is a minimum value of  $R_r$  that comes about when the effect of the inductance  $L_r$  is included. Without the resistance, the circuit is underdamped; the reset voltage oscillates. The behavior of the  $LC$  circuit with saturable core inductor is complex; depending on the magnetic flux in the core following the voltage pulse and the charge voltage on the reset circuit, the core may remain with flux anywhere between  $+B_r$  and  $-B_r$  after the reset. Thus, it is important to ensure that reset current flows only in the proper direction. The optimum choice of  $R_r$  leads to a critically damped reset circuit:

$$R_s \gg 2 \sqrt{L_r/C_r}, \quad (10.16)$$

when Eq. (10.16) is satisfied, the circuit generates a unidirectional pulse with maximum output current.

The following example illustrates typical parameters for an induction cavity and reset circuit. An induction linear accelerator cavity supports a 100-kV, 1- $\mu$ s pulse. The beam current is 2 kA. The laminated core is constructed of 2-mil silicon steel ribbon. The skin depth for the pulselength in silicon steel is about 0.33 mil. The core is therefore in the saturation wave regime. The available flux change in the laminations is 2.6 T. The radially sectioned core has a length of 8 in. (0.205 m). We assume about 30% of the volume of the isolation cavity is occupied by insulation and power

## Linear Induction Accelerators

straps. Taking into account the required volt-second product, the area of the core assembly is

$$A_c = (10^5 \text{ V})(10^{-6} \text{ s})/(0.7)(2.6 \text{ T}) = 0.055 \text{ m}^2.$$

If the inner radius of the core assembly is 6 in. (0.154 m), then the outer radius must be 16.4 in. (0.42 m). These parameters illustrate two features of long-pulse induction accelerators: (1) there is a large difference between  $R_o$  and  $R_i$  so that flux forcing must be used for a good impedance match, and (2) the cores are large. The mass of the core assembly in this example (excluding insulation) is 544 kG. The beam impedance is 50  $\Omega$ . Assume that the damping resistor is 25  $\Omega$  and the charge voltage on the reset circuit is 1000 V. Equation (10.14) implies that

$$C_r > (0.1 \text{ V-s})/(30 \Omega)(1000 \text{ V}) = 3.3 \mu\text{F}.$$

We choose  $C_r = 10 \mu\text{F}$ ; the core is reverse saturated 120  $\mu\text{s}$  after closing the isolation relay. The capacitor voltage at this time is 670 V. Referring to the hysteresis curve of Figure 5.13, the required reset current is 670 A. This implies that  $R_d < 1 \Omega$ . Assuming that the parasitic inductance of the reset circuit is about 1  $\mu\text{H}$ , the resistance for a critically damped circuit is 0.632  $\Omega$ ; therefore, the reset circuit is overdamped, as required.

A convenient method of core reset is possible for short-pulse induction cavities driven by pulse-charged Blumlein line modulators. In the system of Figure 10.18a, a Marx generator is used to charge an oil- or water-filled Blumlein line. The Blumlein line provides a flat-top voltage pulse to a ferrite or Metglas core cavity. A gas-filled spark gap shorts the intermediate conductor to the outer conductor to initiate the pulse. In this configuration, the intermediate conductor is charged negative for a positive output pulse. The crux of the auto-reset process is to use the negative current flowing from the center conductor of the Blumlein line during the pulse-charge cycle to reset the core. Reset occurs just before the main voltage pulse. Auto-reset eliminates the need for a separate reset circuit and high-voltage isolator. A further advantage is that the core can be driven to  $-B_s$  just before the pulse.

Figure 10.18b shows the main circuit components. The impulse generator has capacitance  $C_g$  and inductance  $L_g$ . It has an open circuit voltage of  $-V_0$ . If the charge cycle is long compared to an electromagnetic transit time, the inner and outer parts of the Blumlein line can be treated as lumped capacitors of value  $C_l$ . The outer conductor is grounded; the inner conductor is connected to ground through the induction cavity. We assume there is a damping resistor  $R_d$  that shunts some of the reset current. We will estimate  $V_c(t)$  (the negative voltage on the core during the charge cycle) and determine if the quantity  $\int V_c dt$  exceeds the volt-second product of the core.

Assume that  $V_c(t)$  is small compared to the voltage on the intermediate conductor. In this case, the voltage on the intermediate conductor is approximated by Eq. (9.102) with  $C_2 = 2C_l$ . Assuming that  $C_g = 2C_l$  the voltage on the intermediate conductor is

## Linear Induction Accelerators

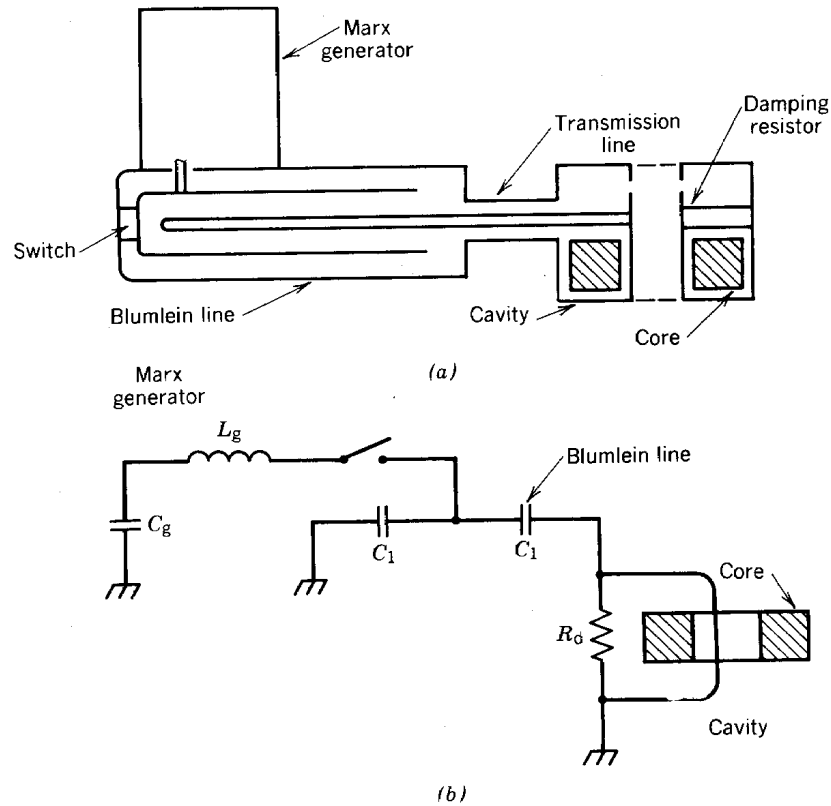


**Figure 10.18** Auto-reset in an induction cavity driven by a Blumlein line. (a) System geometry. (b) Equivalent circuit.

$$V_2 = [V_0 (1 - \cos\omega t)]/2, \quad (10.17)$$

where  $\omega = 1/\sqrt{L_g C_1}$ . The charging current to the cavity is  $i_c \cong C_1 (dV_2/dt)$ . Assuming most of this current flows through the damping resistor, the reset voltage on the core during the Blumlein line charge is

$$V_c \cong - (V_0/2) (R_d / \sqrt{L/C_1}) \sin\omega t. \quad (10.18)$$

If the Blumlein is triggered at the time of completed energy transfer,  $t = \pi/\omega$ , then the volt-second integral during the charge phase is

$$\int V_c dt = V_0 (C_1 R_d). \quad (10.19)$$

## Linear Induction Accelerators

The integral of Eq. (10.19) must exceed the volt-second product of the core for successful reset. This criterion can be written in a convenient form in terms of  $\Delta t_p$ , the length of the main voltage pulse in the cavity. Assuming a square pulse of magnitude  $V_0$ , the volt-second product of the core should be  $V_0 \Delta t_p$ . Substituting this expression in Eq. (10.19) gives the following condition:

$$\Delta t_p \leq C_1 R_d. \quad (10.20)$$

Furthermore, we can use Eq. (9.89) to find the pulselength in terms of the line capacitance. Equation (10.20) reduces to the following simple criterion for auto-reset:

$$Z_1 \leq R_d. \quad (10.21)$$

The quantity  $Z_1$  is the net output impedance of the Blumlein line, equal to twice the impedance of the component transmission lines. Clearly, Eq. (10.21) is always satisfied.

In summary, auto-reset always occurs during the charge cycle if (1) the Marx generator is matched to the Blumlein line, (2) the core volt-second product is matched to the output voltage pulse, and (3) the Blumlein line impedance is matched to the combination of beam and damping resistor. Reset occurs earlier in the charge cycle as  $R_d$  is increased. The condition of Eq. (10.21) holds only for the simple circuit of Figure 10.18. More complex cases may occur; for instance, in some accelerators the cavity and Blumlein line are separated by a long transmission line which acts as a capacitance during the charge cycle. Premature core saturation shorts the reset circuit and can lead to voltage reversal on the connecting line. The resulting negative voltage applied to the cavity subtracts from the available volt-second product.

Flat voltage waveforms are usually desirable. In electron accelerators, voltage control assures an output beam with small energy spread. Voltage waveform shaping is essential for induction accelerators used for nonrelativistic particles. In this case, a rising voltage pulse is required for longitudinal beam confinement (see Section 13.5). Power is usually supplied from a pulse modulator which generates a square pulse in a matched load. There are two primary causes of waveform distortion: (1) beam loading and (2) transformer droop. We will concentrate on transformer droop in the remainder of this section.

The equivalent circuit of an induction linear accelerator cavity is shown in Figure 10.19a. The driving modulator maintains constant voltage if the current to the cavity is constant. Current is divided between the beam load, the damping resistor, and the leakage inductance. The leakage current increases with time; therefore, the cavity does not present a matched load at an times and the voltage droops. The goal is to compensate leakage current by inserting an element with a rising impedance.

A simple compensation circuit is shown in Figure 10.19b. A series capacitor is added to the damping resistor so that the impedance of the damping circuit rises with time. We can estimate the value of capacitance that must be added to keep  $V_0$  constant by making the following



## Linear Induction Accelerators

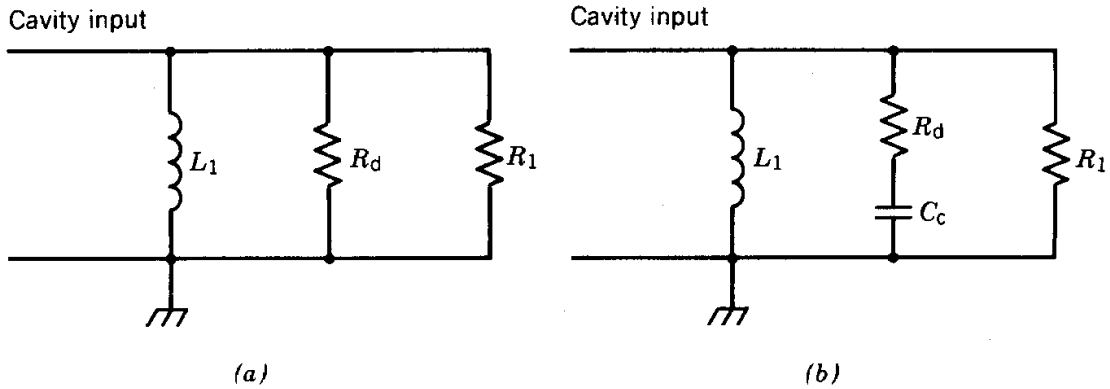


**Figure 10.19** Compensation of voltage droop in an induction cavity. (a) Equivalent circuit of cavity with damping resistor  $R_d$ , no compensation. (b) Simple compensation circuit.

simplifying assumptions: (1) the leakage path inductance is assumed constant over the pulselength,  $\Delta t_p$ ; (2) the voltage on the compensation capacitor  $C_c$  is small compared to  $V_0$ ; (3) the leakage current is small compared to the total current supplied by the modulator; and (4) the beam current is constant. The problem resolves into balancing the increase in leakage current by a decrease in damping current.

With the above assumptions, the time-dependent leakage current is

$$i_1 \cong V_0 t / L_1 \quad (10.22)$$

for a voltage pulse initiated at  $t = 0$ . The current through the damping circuit is approximately

$$i_d \cong (V_0 / R_d) (1 - t / R_d C_d). \quad (10.23)$$

Balancing the time-dependent parts gives the following condition for constant circuit current:

$$R_d C_c = L_1 / R_d. \quad (10.24)$$

As an example, consider the long-pulse cavity that we have already discussed in this section. Taking the average value of  $\mu/\mu_0$  as 10,000 and applying Eq. (9.15), the inductance of the leakage path for ideal ferromagnetic material is

$$L_1 = (\mu/\mu_0) (\mu_0/2\pi) d \ln(R_o/R_i) \cong 400 \mu H.$$

The core actually operates in the saturation regime with a skin depth about one-third the half-thickness of the lamination; we can make a rough estimate of the leakage current by dividing the inductance by three,  $L_1 = 133 \mu H$ . With a damping resistance of  $R_d = 30 \Omega$  and a cavity voltage of 100 kV, the modulator supplies a current greater than 5.3 kA. The leakage current is

## Linear Induction Accelerators

maximum at the end of the pulse. Equation (10.22) implies that  $i_l = 0.25$  kA at  $t = \Delta t_p$ , so that the third assumption above is valid. The compensating capacitance is predicted from Eq. (10.24) to be  $C_c = 0.15$   $\mu$ F. The maximum voltage on the capacitor is 22 kV: thus, assumption 2 is also satisfied. Capacitors are generally available in the voltage and capacitance range required, so that the compensation method of Figure 10.19 is feasible.

### 10.6 INDUCTION CAVITY DESIGN: FIELD STRESS AND AVERAGE GRADIENT

At first glance, it is difficult to visualize the distribution of voltage in induction cavities because electrostatic and inductive electric fields act in concord. In order to clarify field distributions, we shall consider the specific example of the electron injector illustrated in Figure 10.20. The configuration is the most complex one that would normally be encountered in practice. It has

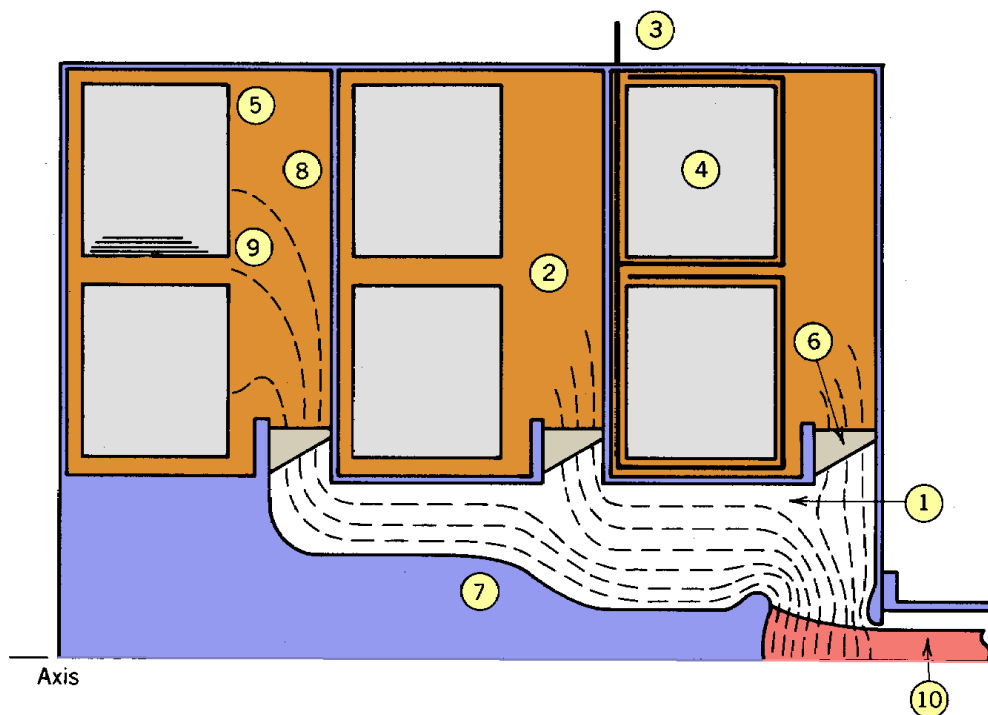


**Figure 10.20** Equipotential lines in six-core injector cavity with radial and longitudinal stacking. (1) Vacuum region, acceleration gap. (2) Transformer oil insulation. (3) Insulated power feed. (4) Laminated isolation core. (5) Exposed face of laminated core. (6) Vacuum insulator with optimized shaping. (7) Shaped negative high-voltage electrode with electron source. (8) Grounded face of laminated core. (9) Location of equipotential line at voltage  $V_0$  with respect to outer wall when flux-forcing straps used. (10) Extracted electron beam.

## Linear Induction Accelerators

laminated cores, longitudinal stacking, radial stacking, and flux-forcing straps. We shall develop an electric field map for times during which all core laminations are unsaturated. In the following discussion, bracketed numbers are keyed to points in the figure.

1. Three cavities are combined to provide 3:1 longitudinal voltage step-up. The load circuit region (1) is maintained at high vacuum, for electron transport. The leakage circuit region (2) is filled with transformer oil for good insulation of the core and high-voltage leads. The vacuum insulator (6) is shaped for optimum resistance to surface breakdown.
2. Power is supplied through transmission lines entering the cavity radially (3). At least two diametrically opposed lines should be used in each cavity. Current distribution from a single power feed has a strong azimuthal asymmetry. If a single line entered from the top, the magnetic field associated with load current flow would be concentrated at the top, causing a downward deflection of the electron beam.
3. The cores (4) are constructed by interleaving continuous ribbons of ferromagnetic material and insulator; laminations are orientated as shown in Figure 10.20. One of the end faces (5) must be exposed; otherwise, the cavity will be shorted by conduction across the laminations.
4. If  $V_0$  is the matched voltage output of the modulator, a single cavity produces a voltage  $2V_0$ . Equipotential lines corresponding to this voltage pass through the vacuum insulator (6). At radii inside the vacuum insulator, the field is electrostatic. The inner vacuum region has coaxial geometry. To an observer on the center conductor (7), the potential of the outer conductor appears to increase by  $2V_0$  crossing each vacuum insulator from left to right.
5. Equipotential lines are sketched in Figure 10.20. In the vacuum region, an equal number of lines is added at each insulator. The center conductor is tapered to minimize the secondary inductance and to preserve a constant field stress on the metal surfaces.
6. In the core region, the electric field is the sum of electrostatic and inductive contributions. We know that the two types of fields cancel along the shorted wall (8). We have already discussed the distribution of equipotential lines inside the core in Section 10.2, so we will concentrate on the potential distribution on the exposed face (5). The inclusion of flux-forcing straps ensures that the two cores in each subcavity enclose equal flux. This implies that the point marked (9) between the cores is at a relative potential  $V_0$ .
7. Each lamination in the cores isolates a voltage proportional to the applied magnetic field  $B_1(r)$ . Furthermore, electrostatic fields in the core are radial. Therefore, the electric field along the exposed face of an individual core has a  $1/r$  variation, and potential varies as  $\Phi(r) \sim \ln(r)$ . The electrostatic potential distribution in the oil insulation has been sketched by connecting equipotential lines to the specified potential on the exposed core surface (5).

## Linear Induction Accelerators

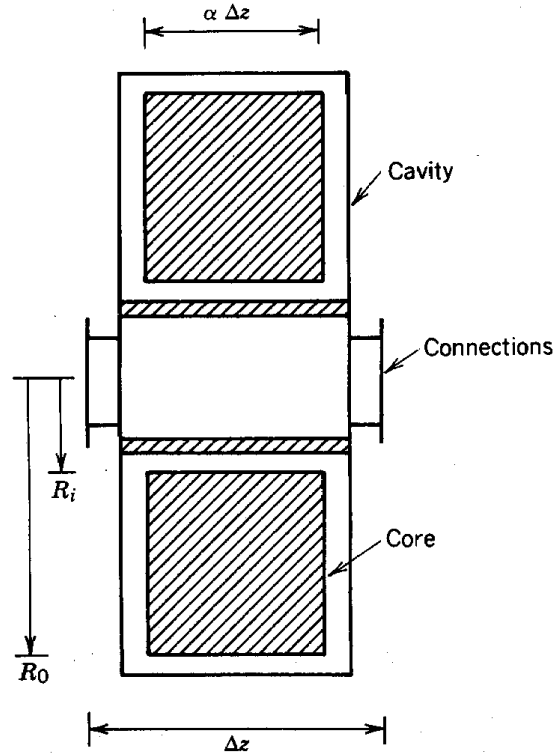


**Figure 10.21** Geometric parameters for calculation of average gradient of linear induction accelerator.

In summary, although the electric field distribution in compound inductive cavities is complex, we can estimate it by analyzing the problem in parts. The distribution could be determined exactly with a computer code to solve the Laplace equation in the presence of dielectrics. There is a specified boundary condition on  $\phi$  along the core face. It should be noted that the above derivation gives, at best, a first-order estimate of field distributions. Effects of core nonlinearities and unequal saturation complicate the situation considerably.

Average longitudinal gradient is one of the main figures of merit of an accelerator. Much of the equipment associated with a linear accelerator, such as the accelerator tunnel, vacuum systems, and focusing system power supplies, have a cost that scales linearly with the accelerator length. Thus, if the output energy is specified, there is an advantage to achieving a high average gradient. In the induction accelerator, the average gradient is constrained by the magnetic properties and geometry of the ferromagnetic core. Referring to Figure 10.21, assume the core has inner and outer radii  $R_i$  and  $R_o$ , and define  $\kappa$  as the ratio of the radii,  $\kappa = R_o/R_i$ . The cavity has length  $\Delta z$  of which the core fills a fraction  $\alpha$ . If particles gain energy  $\Delta E$  in eV in a cavity with pulse length  $t_p$ , the volt-second constraint implies the following difference equation:

$$\Delta E t_p = \Delta B (R_o - R_i) \alpha \Delta z. \quad (10.25)$$

## Linear Induction Accelerators

where  $\Delta B$  is the volume-averaged flux change in the core. The pulselength may vary along the length of the machine; Eq. (10.25) can be written as an integral equation:

$$\int_{E_i}^{E_f} dE t_p(E) = \alpha \Delta B R_o (\kappa-1) L, \quad (10.26)$$

where  $E_f$  is the final beam energy in electron volts,  $E_i$  is the injection energy, and  $L$  is the total length. Accelerators for relativistic electrons, have constant pulselength. Equation (10.26) implies that

$$(E_f - E_i)/L = \alpha \Delta B R_o (\kappa-1) / \Delta t_p \text{ (V/m)}. \quad (10.27)$$

In proposed accelerators for nonrelativistic ion beams [see A, Fattens, E. Hoyer, and D. Keefe, **Proc. 4th Intl. Conf. High Power Electron and Ion Beam Research and Technology**, (Ecole Polytechnique, 1981), 751], the pulselength is shortened as the beam energy is raised to maintain a constant beam length and space charge density. One possible variation is to take the pulselength inversely proportional to the longitudinal velocity:

$$t_p(E) = t_{pf} \sqrt{E_f / E(z)}. \quad (10.28)$$

The quantity  $t_{pf}$  is the pulselength of the output beam. Inserting Eq. (10.28) into Eq. (10.26) gives

$$\left( E_f - \sqrt{E_f E_i} \right) / L = \alpha \Delta B R_o (\kappa-1) / 2t_{pf} \quad (10.29)$$

In the limit that  $E_i \ll E_f$ , the expressions of Eqs. (10.27) and (10.29) are approximately equal to the average longitudinal gradient. In terms of the quantities defined, the total volume of ferromagnetic cores in the accelerator is

$$V = \pi (\kappa^2-1) \alpha L R_o^2. \quad (10.30)$$

Equations (10.27), (10.29), and (10.30) have the following implications:

1. High gradients are achieved with a large magnetic field swing in the core material ( $\Delta B$ ) and the tightest possible core packing  $\alpha$ .
2. The shortest pulselength gives the highest gradient. Properties of the core material and the inductance of the pulse modulators determine the minimum  $t_p$ . High-current ferrite accelerators have a minimum practical pulselength of about 50 ns. The figure is about 1  $\mu$ s for silicon steel

## Linear Induction Accelerators

cores and 100 ns for Metglas cores with thin laminations. Because of their high flux swing and fast pulse response, Metglas cores open new possibilities for high-gradient-induction linear accelerators.

3. The average gradient is maximized when  $\kappa$  approaches infinity. On the other hand, the net core volume is minimized when  $L$  approaches infinity. There is a crossover point of minimum accelerator cost at certain values of  $\kappa$  and  $L$ , depending on the relative cost of cores versus other components.

Substitution of some typical parameters in Eq. (10.27) will indicate the maximum gradient that can be achieved with a linear induction accelerator. Take  $t_p = 100$  ns pulse and a Metglas core with  $\Delta B = 2.5$  T,  $R_i = 0.1$  in and  $R_o = 0.5$  m. Vacuum ports, power feeds, and insulators must be accommodated in the cavity in addition to the cores; we will take  $\alpha = 0.5$ . These numbers imply a gradient of 5 MV/m. This gradient is within a factor of 2-4 of those achieved in rf linear electron accelerators. Higher gradients are unlikely because induction cavities have vacuum insulators exposed to the full accelerating electric fields.

## 10.7 CORELESS INDUCTION ACCELERATORS

The ferromagnetic cores of induction accelerator cavities are massive, and the volt-second product limitation restricts average longitudinal gradient. There has been considerable effort devoted to the development of linear induction accelerators without ferromagnetic cores [A. I. Pavlovskii, A. I. Gerasimov, D. I. Zenkov, V. S. Bosamykin, A. P. Klementev, and V. A. Tananakin, *Sov. At. Eng.* **28**, 549 (1970)]. These devices incorporate transmission lines within the cavity. They achieve inductive isolation through the flux change accompanying propagation of voltage pulses through the lines.

In order to understand the coreless induction cavity, we must be familiar with the radial transmission line (Fig. 10.22). This geometry has much in common with the transmission lines we have already studied except that voltage pulses propagate radially. Consider the conical section electrode as the ground conductor and the radial plate is the center conductor. The structure has minimum radius  $R_i$ . We take the inner radius as the input point of the line. If voltage is applied to the center conductor, a voltage pulse travels outward at a velocity determined by the medium in the line. The voltage pulse maintains constant shape. If the line extends radially to infinity, the pulse never returns. If the line has a finite radius ( $R_o$ ), the pulse is reflected and travels back to the center.

It is not difficult to show that the structure of Figure 10.22 has constant characteristic impedance as a function of radius. (In other words, the ratio of the voltage and current associated with a radially traveling pulse is constant.) In order to carry out the analysis, we assume that  $\alpha$ , the angle of the conical electrode, is small. In this case, the electric field lines are primarily in the axial direction. There is a capacitance per unit of length in the radial direction given by

## Linear Induction Accelerators

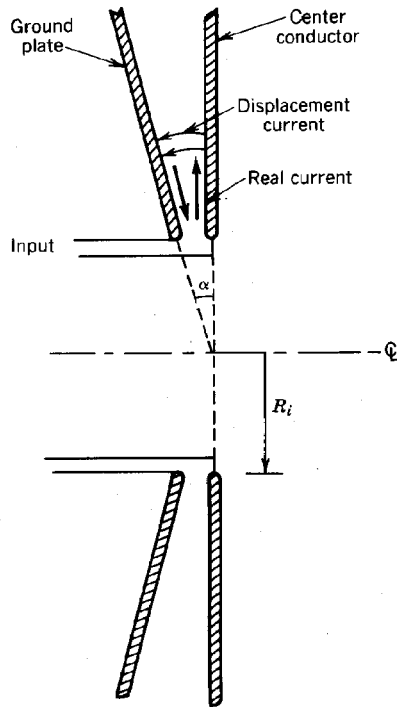


**Figure 10.22** Current flow in radial transmission line.

$$c\Delta r \cong (2\pi r \Delta r)\epsilon / r \tan\alpha = (2\pi\epsilon/\tan\alpha) \Delta r. \quad (10.31)$$

In order to determine the inductance per unit of radial length, we must consider current paths for the voltage pulse. Inspection of Figure 10.22 shows that current flows axially through the power feed, outward along the radial plate, and axially back across the gap as displacement current. The current then returns along the ground conductor to the input point. If the pulse has azimuthal symmetry, the only component of magnetic field is  $B_\theta$ . The toroidal magnetic field is determined by the combination of axial feed current, axial displacement current, and the axial component of ground return current. Radial current does not produce toroidal magnetic fields. The combination of axial current components results in a field of the form

$$B_\theta = \mu I / 2\pi r \quad (10.32)$$

confined inside the transmission line behind the pulse front. The region of magnetic field expands as the pulse moves outward, so there is an inductance associated with the pulse. The magnetic field energy per element of radial section length is

$$U_m dr = (B_\theta^2 / 2\mu) (2\pi r dr) (r \tan\alpha) = \mu I^2 \tan\alpha dr / 4\pi. \quad (10.33)$$



## Linear Induction Accelerators

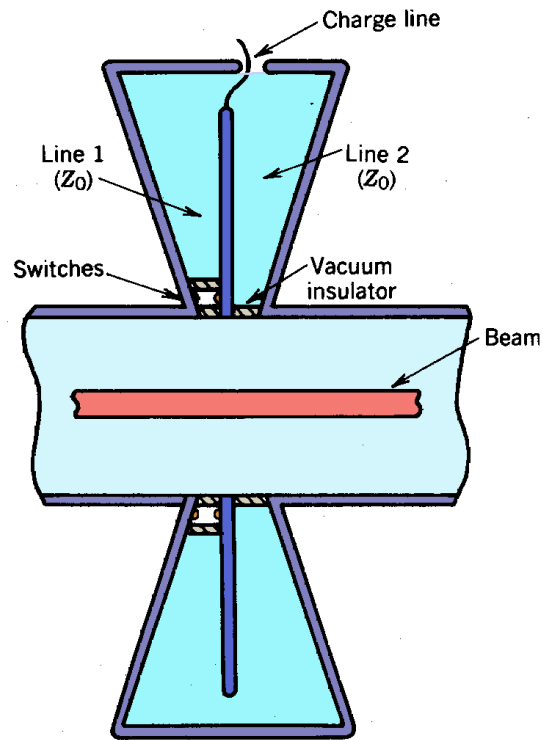


**Figure 10.23** Coreless induction cavity.

This energy is equal to  $\frac{1}{2}lI^2dr$ , so that

$$l = \mu \tan\alpha/2\pi. \quad (10.34)$$

To summarize, both the capacitance and inductance per radial length element are constant. The velocity of wave propagation is

$$v = 1/\sqrt{lc} = 1/\sqrt{\epsilon\mu}. \quad (10.35)$$

as expected. The characteristic impedance is

$$Z_o = \sqrt{l/c} = (\tan\alpha/2\pi) \sqrt{\mu/\epsilon}. \quad (10.36)$$

For purified water dielectric, Eq. (10.34) becomes

$$Z_o = 3.4 \tan\alpha \text{ } (\Omega). \quad (10.37)$$

## Linear Induction Accelerators

The basic coreless induction cavity of Figure 10.23 is composed of two radial transmission lines. There are open-circuit terminations at both the inner and outer radius; the high-voltage radial electrode is supported by insulators and direct current charged to high voltage. The region at the outer radius is shaped to provide a matched transition; a wave traveling outward in one line propagates without reflection through the transition and travels radially inward down the other line. There is a low-inductance, azimuthally symmetric shorting switch in one line at the inner radius. The load is on the axis. We assume, initially that the load is a resistor with  $R = Z_0$ ; subsequently, we will consider the possibility of a beam load which has time variations synchronized to pulses in the cavity.

The electrical configuration of the coreless induction cavity is shown schematically in Figure 10.24a. Because the lines are connected at the outer radius, we can redraw the schematic as a single transmission of length  $2(R_o - R_i)$  that doubles back and connects at the load, as in Figure 10.24b. The quantity  $\Delta t$  is the transit time for electromagnetic pulses through both lines, or

$$\Delta t = 2 (R_o - R_i)/v. \quad (10.38)$$

The charging feed, which connects to a Marx generator, approximates an open circuit during the fast output pulse of the lines. Wave polarities are defined with respect to the ground conductor; the initial charge on the high-voltage electrode is  $+V_0$ . As in our previous discussions of transmission lines, the static charge can be resolved into two pulses of magnitude  $\frac{1}{2}V_0$  traveling in opposite directions, as shown. There is no net voltage across the load in the charged state.

Consider the sequence of events that occurs after the switch is activated at  $t = 0$ .

1. The point marked *A* is shorted to the radial electrode. During the time  $0 < t < \Delta t$ , the radial wave traveling counterclockwise encounters the short circuit and is reflected with reversed polarity. At the same time, the clockwise pulse travels across the short circuit and backward through the matched resistance, resulting in a voltage  $-\frac{1}{2}V_0$  across the load. Charged particles gain an energy  $\frac{1}{2}qV_0$  traveling from point *A* to point *B*. The difference in potential between *A* and *B* arises from the flux change associated with the traveling pulses.

2. At time  $t = \Delta t$ , the clockwise-going positive wave is completely dissipated in the load resistor. The head of the reflected negative wave arrives at the load. During the time  $\Delta t < t < 2\Delta t$ , this wave produces a positive voltage of magnitude  $\frac{1}{2}V_0$  from point *B* to point *A*. The total waveform at the load is shown in Figure 10.25a.

The bipolar waveform of Figure 10.25a is clearly not very useful for particle acceleration. Only half of the stored energy can be used. Better coupling is achieved by using the beam load as a switched resistor. The beam load is connected only when the beam is in the gap. Consider the following situation. The beam, with a current  $V_0/2Z_0$ , does not arrive at the acceleration gap until time  $\Delta t$ . In the interval  $0 < t < \Delta t$  the gap is an open circuit. The status of the reflecting waves is illustrated in Figure 10.24c. The counterclockwise wave reflects with inverted polarity; the clockwise wave reflects from the open circuit gap with the same polarity. The voltage from *B* to *A*

## Linear Induction Accelerators

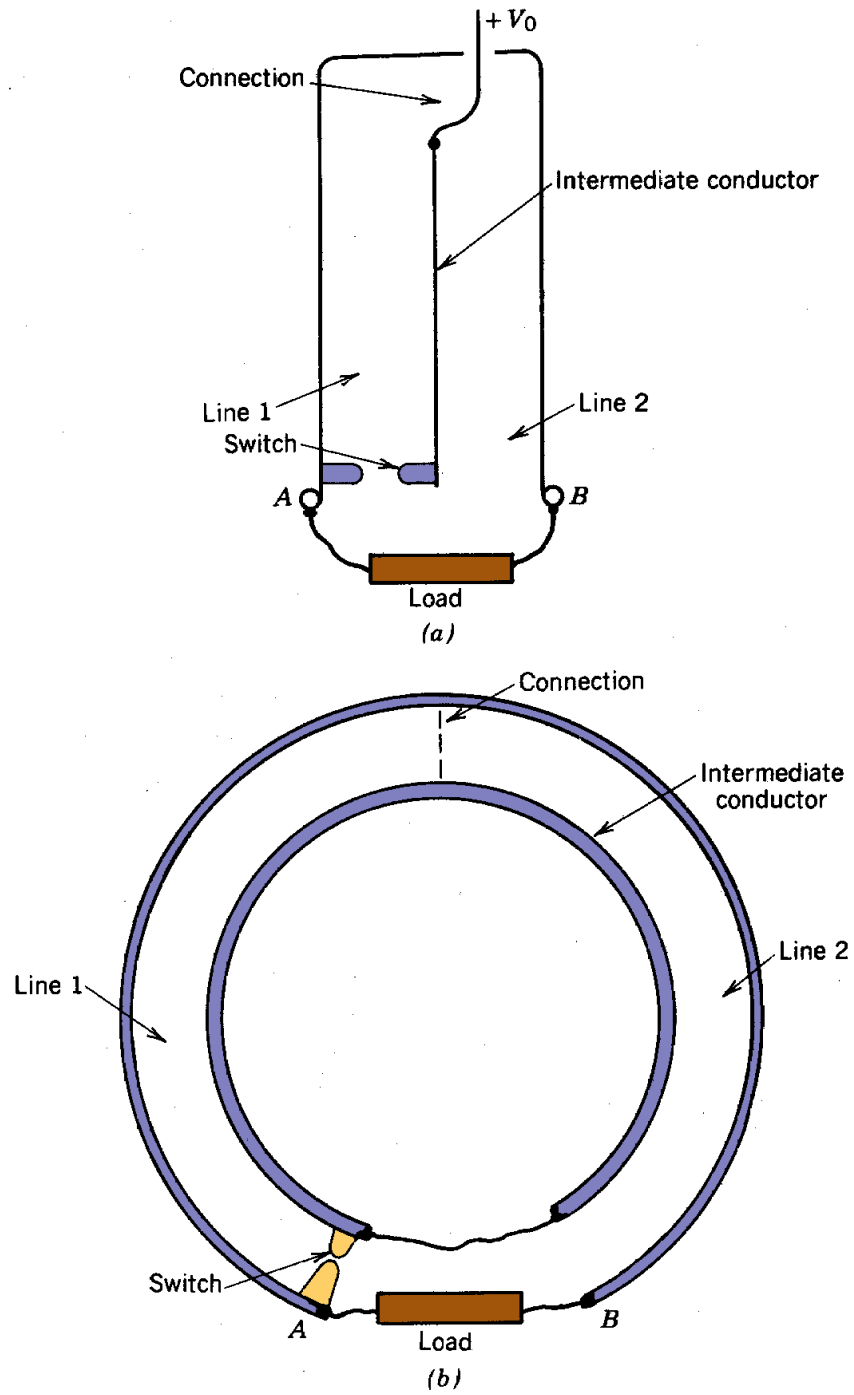
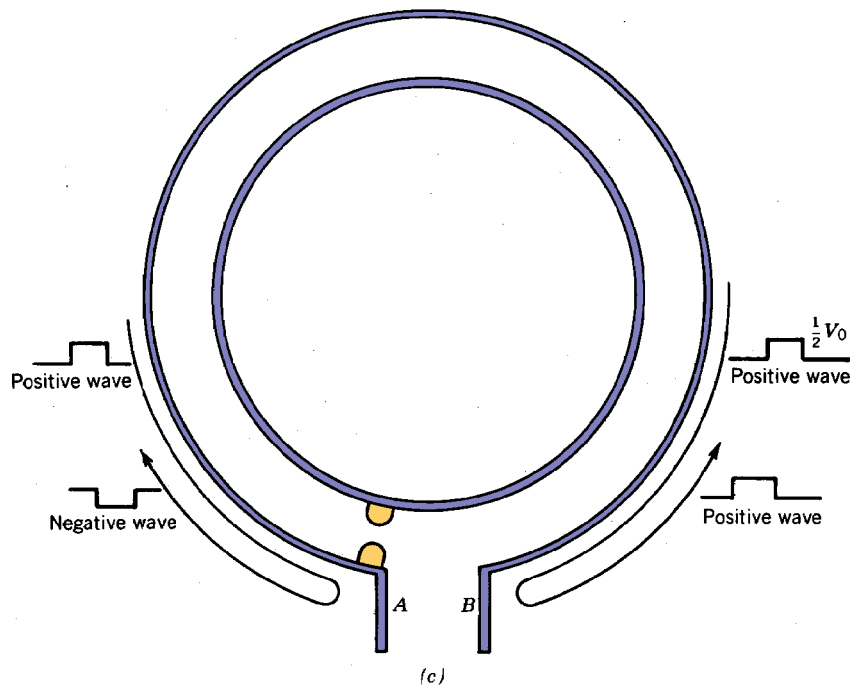


**Figure 10.24** Coreless induction cavity. (a) Simplified geometry. (b) Equivalent geometry with ideal outer connection between lines. (c) Resolution of static charge into traveling square pulses; polarity and propagation direction of pulses immediately following switch shorting.

## Linear Induction Accelerators



(c)  
Figure 10.24 (Continued).

is the open-circuit voltage  $V_0$ . At time  $t = \Delta t$ , both the matched beam and the negative wave arrive at the gap. The negative wave makes a positive accelerating voltage of magnitude  $\frac{1}{2}V_0$  during the time  $\Delta t < t < 2\Delta t$ . In the succeeding time interval,  $2\Delta t < t < 3\Delta t$ , the other wave which has been reflected once from the open-circuit termination and once from the short-circuit termination arrives at the gap to drive the beam. The waveform for this sequence is illustrated in Figure 10.25b. In theory, 100% of the stored energy can be transferred to a matched beam load at voltage  $\frac{1}{2}V_0$  for a time  $2\Delta t$ .

Although coreless induction cavities avoid the use of ferromagnetic cores, technological difficulties make it unlikely that they will supplant standard configurations. The following problems are encountered in applications:

1. The pulselength is limited by the electromagnetic transit time in the structure. Even with a high dielectric constant material such as water, the radial transmission lines must have an outer diameter greater than 9 ft for an 80-ns pulse.
2. Energy storage is inefficient for large-diameter lines. The maximum electric field must be chosen to avoid breakdown at the smallest radius. The stored energy density of electric fields [Eq. (5.19)] decreases as  $1/r^2$  moving out in radius.

## Linear Induction Accelerators

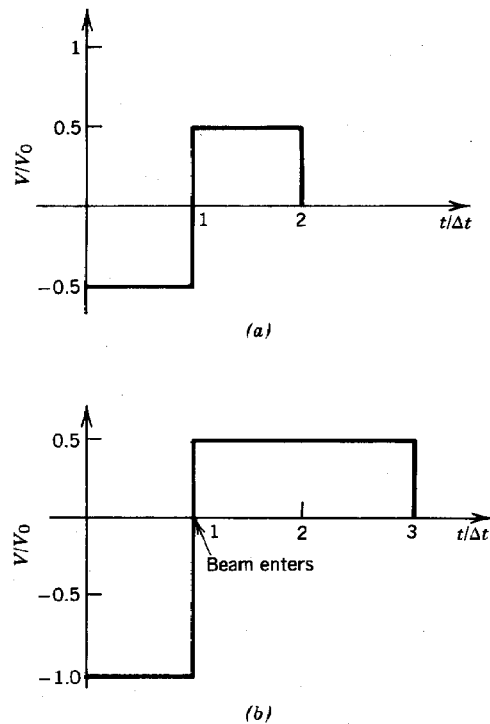


**Figure 10.25** Voltage waveform in coreless induction cavity. (a) Simple matched load resistor. (b) Synchronized beam load with matched impedance.

3. Synchronous low-inductance switching at high voltage with good azimuthal symmetry is difficult.
4. Parasitic inductance in the load circuit tends to be larger than the primary inductance of the leakage path because the load is a beam with radius that is small compared to the radius of the shorting switches. The parasitic inductance degrades the gap pulse shape and the efficiency of the accelerator.
5. The switch sequence for high-efficiency energy transfer means that damping resistors cannot be used in parallel with the gap to protect the cavity.
6. The vacuum insulators must be designed to withstand an overvoltage by a factor of 2 during the open-circuit phase of wave reflection.

One of the main reasons for interest in coreless induction accelerators was the hope that they could achieve higher average accelerating gradients than ferromagnetic cavity accelerators. In fact, a careful analysis shows that coreless induction accelerators have a significant disadvantage in terms of average gradient compared to accelerators with ferromagnetic isolation. We will make the comparison with the following constraints:

## Linear Induction Accelerators

1. The cavities have the same pulselength  $\Delta t_p$  and beamcurrent  $I_o$ .
2. Regions of focusing magnets, pumping ports, and insulators are not included.
3. The energy efficiency of the cavities is high.

We have seen in Section 10.6 that the gradient of an ideal cavity with ferromagnetic isolation of length  $l$  with core outer radius  $R_o$  and inner radius  $R_i$  is

$$V_o/l = \Delta B (R_o - R_i) / \Delta t_p. \quad (10.39)$$

where  $\Delta B$  is the maximum flux swing. Equation (10.39) proceeds directly from the volt-second limitation on the core. In a radial line cavity, the cavity length is related to the outer radius of the line,  $R_o$ , by

$$l = 2 R_o \tan \alpha, \quad (10.40)$$

where  $\alpha$  is the angle of the conical transmission lines. The voltage pulse in a high-efficiency cavity with charge voltage  $V_o$  has magnitude  $1/2 V_o$  and duration

$$\tau_p = 4 (R_o - R_i) \sqrt{\epsilon/\epsilon_o}/c, \quad (10.41)$$

where  $R_i$  is the inner radius, of the transmission lines. We further require that the beam load is matched to the cavity:

$$Z_o = V_o/2I_o.$$

The characteristic impedance is given by Eq. (10.36). Combining Eq. (10.36) with Eqs. (10.40) and (10.41) gives the following expression for voltage gradient:

$$V_o/l = (\mu_o/\pi) (1 - R_i/R_o) I_o / \Delta t_p.$$

Equation (10.42) has some interesting implications for coreless induction cavities. First, gradient in an efficient accelerator is proportional to beam current. Second, the gradient for a given pulselength is relatively insensitive to the outer radius of the line. This reflects the fact that the energy storage density is low at large radii. Third, the gradient for ideal cavities does not depend on the filling medium of the transmission lines. Within limits of practical construction, an oil-filled line has the same figure of merit as a water-filled line.

In order to compare the ferromagnetic core and coreless cavities, assume the following conditions. The pulselength is 100 ns and the beam current is 50 kA (the highest current that has presently been transported a significant distance in a multistage accelerator). The ferromagnetic

### Linear Induction Accelerators

core has  $R_o = 0.5$  m,  $R_i = 0.1$  m, and  $\Delta B = 2.5$  T. The coreless cavity has  $R_i/R_o \ll 1$ . Equation (10.39) implies that the maximum theoretical gradient of the Metglas cavity is 10 MV/m, while Eq. (10.42) gives an upper limit for the coreless cavity of only 0.16 MV/m, a factor of 63 lower. Similar results can be obtained for any coreless configuration. Claims for high gradient in coreless accelerators usually are the result of implicit assumptions of extremely short pulselengths (10-20 ns) and low system efficiency.